FACULTY OF GRADUATE STUDIES

Master Program of Applied Chemistry

A Comparative Study of Fe, Cu Nanoparticles and Bimetallic Fe-Cu Nanoparticles in the Removal of Methyl Orange from Water and Water-Ethanol Solutions

دراسة مقارنة بين دقائق الحديد النانوية ودقائق النحاس النانوية والدقائق النانوية المختلطة للحديد والنحاس في إزالة مادة "مثيل أورانج" من محاليل الماء ومحاليل مكونة من الماء والإيثانول

Mayes Jamal Majadleh

1185110

Supervisor: Professor Talal Shahwan

This Thesis was submitted in partial fulfillment of the requirements for the Master's Degree in Applied Chemistry From the Faculty of Graduate Studies at Birzeit University, Palestine

February 2022

A Comparative Study of Fe, Cu Nanoparticles and Bimetallic Fe-Cu Nanoparticles in the Removal of Methyl Orange from Water and Water-Ethanol Solutions

We approve the thesis of Mayes Majadleh

_____

Prof. Talal Shahwan

Supervisor

Chemistry Department- Faculty Member

Birzeit University

_____

Assist. Prof. Saleh Sulaiman

Committee Member

Chemistry Department- Faculty Member

Birzeit University

_____

Assist. Prof. Muhammed Aljabari

Committee Member

Chemistry Department- Faculty Member

Birzeit University

1 February 2022

Acknowledgement

I'd want to express my gratitude to everyone who assisted me throughout the thesis process, starting with my supervisor, Professor Talal Shahwan, who never stopped encouraging me to do a wonderful job; the thesis would not have been completed without his guidance. Thanks for the continuous support and kind communication, which had a great effect regarding to feel interesting about what we worked on.

Thanks are extended to the chemistry department members at Birzeit University represented by its head Dr.Imtiaz Darwish, and lab technicins:, Mr. Asem Mubarak, and Dr. Ibrahim Shalash for their help throughout my thesis experiments. Warm Regards to Mrs. Gader Taim for her kind support and help through my years study.

For the examination committee, Dr. Saleh Sulaiman and Dr. Mohammed Aljabari for their efforts in reading and assessing the thesis.

Many thanks to Dr. Montaha Maser (at Ulm University, Germany) who helped in SEM, EDX, XPS, XRD characterization.

Abstract

Nowadays there are continuously increasing worldwide attempts for the development of wastewater treatment technologies due to increasing pollution caused by anthropogenic activities. Dyes form one of the most familiar groups of water pollutants, which have harmfull effects on the environment and human health. As a result, there is a wide international interest in innovational methods for the removal of dyes from water.

The utilization of nanomaterials for the removal of dyes from water has taken numerous concern due to their special chemical and physical characteristics, like very small size, high surface-area-to-volume ratio, surface modifiability, and other characteristics.

In this study, nanoparticles of zero-valent iron (nZVI), nanoparticles of zero-valent copper (nZVC), and bimetallic iron-copper (Fe-Cu) nanoparticles were prepared by liquid-phase reduction, characterized by different techniques, and used to remove methyl orange (MO) dye from water, water-ethanol, water-DMSO solutions. The experiments investigated the effects of solvent type, nanoparticles type, nanoparticles dosage, the salinity of the solutions, temperature, and shaking time on the extent of MO sorption. Heterogeneous Fenton oxidation reactions were also tested. These experiments were carried out in pure water and water-ethanol solutions basically, in addition to some experiments carried out in water-DMSO solution, in order to assess the effect of solvent type on the efficiency of removal of MO by synthesized NPs.

The results showed that due to the variation in the solvent-solute interactions, very high removal of MO was observed from water solutions, a limited removal was achievable in water-ethanol solutions, and very poor removal was observed in water-DMSO solutions. Therefore, the comparative study was conducted basically between pure water and water-ethanol solvents. On the overall, the efficiency of Fe NPs towards MO removal was higher than that of Cu and Fe-Cu NPs. This study found that increasing the NPs dose results in increasing the removal from water solutions by the three nanoparticle types. In addition, it was found that rising the temperature results in increasing the extent of MO removal from water and water-ethanol solutions by Fe and Fe-Cu NPs, indicating endothermic behavior of the removal process. On the other hand, rising the temperature results in decreasing the removal of MO from water by

Cu NPs indicating exothermic behavior of the process. Also, it was found that adding NaCl salt to the MO solutions has a negative effect on the removal of MO when iron and copper NPs were used.

Moreover, the heterogeneous Fenton process leads to smaller MO removal when it is compared with the directly application of the synthesized nanoparticles, for both water and water-ethanol solutions. The dye removal process from water using Fe NPs was much faster than water-ethanol solutions. The kinetics data showed that the removal of MO from water by Fe NPs follows a pseudo-second order rate equation.

الملخص بالعربية

فِي الْوَقْتِ الْحَاضِـرِ، هُنَاكَ مُحَاوَلَاتٍ مُتَزَايِدَةٍ بِاسْـتِمْرَارٍ فِي جَمِيعِ أَنْحَاءِ الْعَالَمِ لِتَطْوِيرِ تِقْنِيَّاتٍ لِمُعَالِجَةِ المِيَاه بِسَـبَبِ التَّلَوُّثِ الْمُتَزَايِد النَّاجِمِ عَنِ الْأَنْشِـطَةِ الْبَشَـرِيَّةِ. تُشَـكِّلُ الْأَصْـبَاغُ إِحْدَى أَكْثَرِ مَجْمُوعَات مُلَوِّثَات الْمِيَاهَ شُـيُوعًا، والَّتِي لَهَا آثَارُ ضَارَّةُ عَلَى الْبِيئَةِ وَصِـحَّةِ الْإِنْسَانِ، وَنَتِيجَةً لِذَلِكَ هُنَاكَ اِهْتِمَامِ دَوْلِيّ وَاسِعِ بِالطُّرُقِ الْمُبْتَكَرَةِ لِإِزَالَةِ الْأَصْبَاغِ مِنَ الْمَاءِ.

حَظِيَ اِسْتِخْدَامُ الْمَوَادِّ النانوية لِإِزَالَةِ الْأَصْبَاغِ مِنَ الْمَاءِ بِاهْتِمَامِ كَبِيرِ فِي هَذَا الْمَجَالِ نَظَرًا لخصَـائِصـهَا الْكِيمْيَائِيَّةَ وَالْفِيزِيَائِيَّةَ الْفَرِيدَةَ، مِثْلُ الْحَجْمِ الصَّغِيرِ لِلْغَايَةٍ، وَنِسْبَةَ مِسَاحَةِ السَّطْحِ إِلَى الْحَجْمِ الْعَالِيَةِ، وَقَابِلِيَّةَ تَعْدِيلِ السَّطْحِ، وخصائص أُخْرَى.

فِي هَذِهِ الدِّرَاسَـــةِ، تَمَّ تَحْضِـــيرُ دَقَائِقِ الْحَدِيدِ النانوية وَدَقَائِقَ النّحاسِ النانوية وَخَلِيطَ مِنْ دَقَائِقِ الْحَدِيدِ وَالنَّحاسِ مَعًا (ثُنَائِيَّ الْمَعْدِنِ) بَوَاسِطَةَ طَرِيقَةِ الْإِخْتِزَالِ فِي الْحَالَةِ السَّائِلَةِ. وقد تَمّ تَشْخِيصـها بِاسْتِخْدَامِ تِقْنِيَّاتِ عِدَّةٍ، وَتم اسْتَخْدِامُها لِإِزَالَةِ صِـبْغَةً "ميثيل أورانج"مِنْ مَحَالِيلِ الْمَاءِ، الماءوالإيثانول، وَالْمَاءَ وَثُنَائِيَّ ميثل السلفوكسيد.

وَقَدْ تَمَّ دِرَاسَـــةُ تَأْثِيرِ نَوْعِ المذيب وَنَوْعَ الْجَسِـــيمَاتِ النانوية وَكَمِّيَّةَ الدَّقَائِقِ النانوية وَمُلُوحَةَ الْمَحَالِيلِ وَتَأْثِيرِ دَرَجَةِ الْحَرَارَةِ وَالْوَقْت عَلَى مُدَى اِزالة"ميثيل أورانج" .وقد أَجْرَيْتُ هَذِهِ التَّجَارِبِ فِي الْمَاءِ النُّقِيّ وَالمَحَالِيلِ المكونة من الْمَاءِ والايثانول بِشَكْلِ أَسَاسِـيّ، بالإضافة لبَعْضَ التجارب التي أجريت باستخدام مَحَالِيلَ مكونة من الْمَاءِ وَثُنَائِيَّ ميثل السلفوكسيد، مِنْ أَجَلْ تَقْيِيمَ مُدَى تَأْثِيرِ مُحْتَوَى الايثانول عَلَى كَفَاءةِ عَمَلِيَّةِ ازالة صِبْغَةَ ميثيل أورانج.

وَأَظْهَرَتْ نَتَائِجُ هَذِهِ الدِّرَاسَةِ إِنَّهُ نَتِيجَةً لِإِخْتِلَافِ سُلُوكِ الميثيل اورانج بِإِخْتِلَافِ نَوْعِ المذيب فَانِ ازالة هَذِهِ الصِّبْغَةِ مِنَ الْمَاءِ كَانَتْ جَيِّدَةُ بَيْنَمَا كَانَتِ الازالة مَحْدُودَةً فِي حَالَةِ المَحَالِيل المكونة من الْمَاءِ والايثانول وَمَعْدُومَةَ تَقْرِيبًا فِي حَالَةِ المَحَالِيلَ المكونة من الْمَاءِ وَثُنَائِيّ ميثيل السـالفوكسـيد. لِذَلِكَ فَإِنَّ الدِّرَاسَـةَ الْمُقَارنة تَمُتُّ بِشَـكْلِ أَسَـاسِـيّ بَيْنَ الْمَاءِ النُّقِيّ والمحاليل المكوّنة من الْمَاءِ والإيثانول. كَانَتْ كَفَاءةُ دَقَائِقِ الْحَدِيدِ النانوية تُجَاهَ إِزَالَةِ الصِّـــبْغَةِ أَعَلَى مِنْ دَقَائِقِ النَّحَّاسِ النانوية وَخَلِيطَ الْحَدِيدِ وَالنَّحَّاسِ مَعًا. وَوَجَدَتْ هَذِهِ الدِّرَاسَـةِ أَيْضًـا أَنَّ زِيَادَةَ كَمِّيَّةَ الْمَوَادِّ النانوية الْمَحْضَـرَةَ أَدَّتْ إِلَى زِيَادَةِ نِسْـبَةِ الْإِزَالَةِ مِنَ الْمَحَالِيلِ الْمَائِيَّةِ. بِالْإِضَـــافَةِ إِلَى ذَلِكَ، وَجِدٌ أَنَّ اِرْتِفَاعَ دَرَجَةِ الْحَرَّارَةِ يُؤَدِّي إِلَى زِيَادَةِ نِسْـــبَةِ إِزَالَةِ الميثيل أورانج مِنَ الْمَاءِ وَالمَحَالِيلِ المكونة من الإيثانول والْمَاء بَوَاسِـطَةُ دَقَائِقِ الْحَدِيدِ النانوية وَخَلِيطَ الْحَدِيدِ وَالنَّحَّاسِ مَعَا مِمَّا يُشِـيرُ إِلَى السُّـلُوكِ الماص لِلْحَرَارَةِ لِعَمَلِيَّةِ الْإِزَالَةِ فِي هَذِهِ الْحَالَةِ. مِنْ نَاحِيَةِ أُخْرَى، أَدَّى اِرْتِفَاعُ دَرَجَةِ الْحَرَارَةِ إِلَى تَقْلِيلِ نِسْـــبَةِ إِزَالَةِ الميثيل أورانج مِنَ الْمَاءِ بَوَاسِـــطَةَ دَقَائِقِ النَّحَّاسِ النانوية مِمَّا يشـــير الى السُّـــلُوكِ الطَّارِدِ لِلْحَرَارَةِ لِلْعَمَلِيَّةِ فِي حَالَةِ النَّحَّاسِ.

أَيْضًـا، وَجِدٌ أَنَّ إِضَـافَةَ الْمِلْحِ إِلَى مَحَالِيلِ الميثيل أورانج لَهُ تَأْثِيرُ سَـلْبِيُّ عَلَى نِسْبَةِ الْإِزَالَةِ عِنْدَ اِسْتِخْدَامِ دَقَائِقِ الْحَدِيدِ وَدَقَائِقِ النَّحَّاسِ النانوية. عِلَاوَةٌ عَلَى ذَلِكَ، فَإِنَّهُ تَمَّ دِرَاسَةِ التَّفَاعُلِ بِعَمَلِيَّةٍ تُشْبِهُ تَفَاعُلُ " فَيَنْتُوَنَّ " حَيْثُ كَانَتْ نِسْبَةُ ازالة الصِّبْغَةَ قَلِيلَةُ مُقَارَنَة مَعَ مَا تَمَّ الْحُصُـــولِ عَلَيْهِ عِنْدَ اضـــافة دَقَائِقَ الْحَدِيدِ وَدَقَائِقِ النَّحَّاسِ النانوية وَخَلِيطَ الْحَدِيدِ وَالنَّحاسِ مُبَاشِـــرَةَ لِكلا الْمَحَالِيلُ الْمَائِيَّةُ وَالْمُكَوِّنَةُ مِنَ الايثانول وَالْمَاءَ. كَانَتْ عَمَلِيَّةُ إِزَالَةِ الصِّـبْغَةِ مِنَ الْمَاءِ بِاسْـتِخْدَامِ دَقَائِقِ الْحَدِيدِ النانوية أَسْـرَعَ بِكَثِيرِ مِنَ الازالة مِنَ الْمَحَالِيلِ الْمُكَوِّنَةَ مِنَ الإيثانول وَالْمَاء. كَمَا أَظْهَرَتِ النَّتَائِجُ اِنهَ عِنْدَ اِسْتِخْدَامِ دَقَائِقِ الْحَدِيدِ النانوية لِإِزَالَةِ هَذِهِ الصِّبْغَةِ مِنَ الْمَاءِ فَانِ نَمُوذَجِ التَّفَاعُلِ مِنَ الدَّرَجَةِ الثَّانِيَةِ أَفَضْلٌ مَا يَصِفُ حَرَكَةُ هَذَا النِّظَام.

List of Abbreviations

MO	Methyl Orange
nZVI	Nano Zero Valent Iron
nZVC	Nano Zero Valent Copper
NPs	Nanoparticles
W	Water
W-E	Water-Ethanol
DMSO	Dimethyl sulfoxide

Table of Contents

List of Figures

List of Table

1. Introduction

1.1 Water Pollution and Dyes

Environmental pollution is one of the most important issues which confront different life forms on our planet today.[1] The definition of environmental pollution can be abbreviated as, "The contamination of the physical and biological components of the earth/atmosphere system to such an extent that normal environmental processes are adversely affected."[2] There are several sources of environmental pollution including: industrialization, urbanization, population growth, exploration, and mining.[3] Mining activities for example, are posing danger to the environment through releasing of dust, depositing and transporting of heavy metals, polluting water and soil, and health issues.[4] Air, water, and soil/land pollution are the main types of existing pollution.[5]

Water pollution is a global phenomenon and one of the essential issues for many developing nations. Most of this water is untreated and consumed for household effluents, hospitals, industries, etc. So many toxic compounds and other chemicals pollute the water as per a United Nations report.[6] Since water is one of the major elements responsible for life on earth, which is used every day for various purposes, safe water availability is essential for public health.[7] Therefore, water pollution and the scarcity of water resources are motivating world-wide research that aims at finding novel and efficient methods for water purification. The main sources of water contamination are of anthropogenic origin, and include industrial activities (such as dye and pigment industries, textile, pharmaceutical, etc.), agricultural activities, municipal wastewater, and others. Various types of organic pollutants, including dyes, have been found to contaminate water resources. The discharge of dyes into water bodies as industrial wastes is very dangerous, due to their various side effects and embryotoxicity, mutagenicity, teratogenicity, and carcinogenicity as well as health disorders to human beings.[8,9,10]

Dyes and pigments are the most essential colorants, which are usually used to provide a color or change the color of a substrate. These two-colour additives are used in various industries, like in the textiles, pharmaceutical, food, cosmetics, plastics, paint, ink, photographic and paper industries.[11]

The main difference between dyes and pigments refers to their solubility in the medium. While dyes are soluble in water and/or an organic solvent, pigments are insoluble in both types of liquid media. Also, the dispersion of dyes in the substrate is at a molecular level, but pigments are insoluble and are dispersed as particles.[12,13]

Dyes are natural or synthetic-colored compounds that impart permanent color to fabric, leather, wood, *etc*. So, they are among the most broadly used chemical substances in daily life and different industries. Most of the dyes are organic compounds that contain aromatics, amines, and sometimes trace heavy metals like Cd, Cu, Pb, Zn and Co. In particular, every dye molecule contains three parts: chromophores, chromogene, and auxochromes.[13,14]

The dye color is a result of the chromogene-chromophore structure (acceptor of electrons), and the dyeing capacity is due to auxochrome groups (donor of electrons). The chromogene is composed of an aromatic structure normally based on rings of benzene, naphthalene or anthracene, from which are binding chromophores that contain double conjugated links with delocalized electrons. The chromophore part is a covalently unsaturated group, which can absorb UV or visible light. This absorption leads to electronic excitation, and an electron moves to a higher electronic energy level from a lower one. Chromophores include the azo group (-N=N-), ethylene group (=C=C=), methine group (-CH=), carbonyl group (=C=O), carbon-nitrogen (=C=NH; -CH=N-), carbon-sulfur (=C=S; ≡CS-S-C≡), nitro ($-NO_2$; -NO-OH), nitrozo (-N=O; =N-OH) or chinoid groups. The chromophores may or may not give colour to a compound. If a chromophore absorbs radiation in visible region (400-800 nm), the compound will be coloured. But if it absorbs in UV region the compound will be not coloured. Chromophores like C=C or C≡C having π electrons undergo $\pi \rightarrow \pi^*$ transitions and those having both π and non-bonding electrons, e.g., C=O, C≡N or N=N, undergo $\pi \rightarrow \pi^*$, $n \rightarrow \pi^*$ and $n \rightarrow \sigma^*$ transitions. The last constituent of dyes is the auxochrome groups, which are known as covalently saturated ionizable groups, that provide the dyes with the binding capacity onto the textile material. The auxochrome groups include: $-NH_2$ (amino), -COOH (carboxyl), $-SO_3H$ (sulphonate) and -OH (hydroxyl). An auxochrome (also called colour enhancing group) by itself does not represent absorption above 200 nm. But, when it is attached to a chromophore, changing in the wavelength and the intensity of the absorption maximum will occur. Auxochromes generally increase the value of λ_{max} as well as ε_{max} by extending the conjugation through resonance. This combination between chromophore and auxochrome gives like a new chromophore having different values of λ_{max} and ε_{max}.[13,15]

There are many types of dyes, which are classified based on their application (like azoic, direct, disperse, etc.) and based on chemical structure (like azo, nitro, nitroso, diarylmethane, etc.). In addition, they are classified into neutral, cationic and anionic dyes according to the charge over the organic dyes. [16,17] In the early twentieth century, synthetic dyes had large dominancy over natural ones, due to their attractive properties like simple synthesis, coloring in good quality, and broad application.[18] At the same time, due to the harmful effects of these dyes, it is necessary to use and develop effective and economic dye effluent treatment processes.[19]

1.2 Methods for Dye Removal

It is estimated that half of the worldwide synthetic dyes are non-biodegradable and have carcinogenic effects.[20] They are not degraded by light or heat or natural oxidants due to their high thermal and chemical stability.[21] So the removal of these colorants from wastewater is extremely essential. In order to avert the harmful accumulation of dyes in the water, it's important to improve efficacious ways for the removal of these pollutants from wastewater.[22]

Traditionally, physical, chemical, electrical, and biological methods are used for wastewater treatment, and this applies to dyes as an important category of pollutants. However, in literature, it is reported that using one of these methods alone may lead to color removal from water, but at the same time, can lead to keeping hazardous organics in the treated water. Thus, both color removal and organic reduction must be considered integrated parts of the overall process evaluation. Therefore, it is important to combine these processes in order to achieve the desirable purposes. [23] This combination between processes is known as a physicochemical treatment.[24] Currently several physicochemical methods are being utilized for dye removal. These methods can be classified into the following three major groups:

(1) Destructive redox methods, which leads to transforming the organic compounds to simpler easily oxidized organic products or mineral compounds. In this group of methods, the usage of ozone (O_3) and hydrogen peroxide (H_2O_2) as oxidizing agents is most promising for environmental reasons, but it is limited by their cost's elevation and large consumption of reagent.[25] The combination between UV light and H_2O_2 for dye decolorization is investigated. In this method, UV light activates the decomposition of the hydrogen peroxide to free radicals' production, mainly hydroxyl radicals, which is responsible for dye degradation by chemical

oxidation of the dyes and organic molecules, leading to the formation of end products like CO_2 and H_2O. These combined techniques are relatively expensive, but they are achieved in less time as compared to other methods when applied individually.[14]

(2) The transfer of pollutants to sediment or floated sludge, coagulation, reagent pressure flotation, and electrocoagulation.[25] Coagulation is one of the widely used physicochemical treatment methods. Most of the time it is used in the pretreatment process to achieve a sufficient removal of the dyes from wastewater, so, decreasing the burden for the later biochemical treatment facilities.[26] In this process, it is not easy to remove dyes that have high solubility in water, and it leads to large quantities of sludge production. As a result, in order to get acceptable effluent color quality, techniques like biological processes are mixed with the coagulation process to get acceptable effluent color quality and efficient removal of dyes. It is reported that when Fe (II) is used in coagulation, the addition of hydrogen peroxide as a Fenton's reagent leads the process to be more effective due to simultaneous oxidation and coagulation.[23]

(3) Separation methods which include traditional sorption on activated carbons and microporous, ion exchange resins, and reverse osmosis.[25] In the case of ion-exchange adsorbents, the pollutants having opposite charges to the adsorbents charge will be binding with this ion-exchange adsorbent. Clay, ion-exchange resins, and lignocellulosic biomasses are examples of ion-exchange adsorbents type. Clay types, particularly those with high iron and aluminum percent, calcined and non-calcined types, have been reported to have removal ability of reactive dyes from wastewater. The higher surface area of calcined clays makes them preferred over non-calcined clays, with better dye binding capacities.[27]

However, all of the conventional methods are having some limitations due to high costs, complicated constructions and removal effectiveness.[28] In contrast, the adsorption method was preferred by most of the researches due to its special properties like simplicity, low costs of construction and maintenance, insensitivity to toxic pollutants, and being a universal method, which has high efficiency toward dyes removal.[29,30,31] The adsorption process depends basically on the surface of adsorbent. In this process, a substance adheres on the surface of adsorbent either by weak intermolecular forces, like van der Waals forces (physical adsorption), or by chemical bonds (chemical adsorption). The reverse process of adsorption is known as the desorption process. In the adsorption process many factors affect the extent of this process like molecular weight of adsorbent, polarity and concentration of solution, surface area and surface charge.[17]

Activated carbon, chitosan and charcoal have been reported to be efficient for dyes' removal from wastewater.[32] Activated carbon which is previously pre-prepared by using carbon from coal, coconut shell, wood etc., through chemical or physical activation methods is one of the oldest adsorbents known. It is widely used as an adsorbent to remove dyes from waste water due to its attractive properties and benefits including high surface area, pore size, easy to design, and high adsorption capacity.[33,34]

Despite the excellent adsorption performance of activated carbon, it is costly and has poor selectivity toward dispersed dyes, therefore many alternatives have been developed to reduce the cost and improve the efficiency of adsorbents, such as clays/zeolites and their composites, biosorbents, and agricultural solid wastes.**[10]** Recently, to overcome difficulties related to cost, efficiency, operational method, and energy needs in dyes wastewater treatments, nanomaterials have been developed and used, and have shown high removal efficiency and low costs requirements.[35] This type of materials is defined as the materials in which one or more external dimensions lies in the range between 1 and 100 nm.[36] Thus nano-adsorbents can be a nanoparticles, nanofibers and nanotubes, nanosheets, and nanoflowers.[37]

Nanomaterials have a large surface area and are usually unique chemical, physical, optical, electrical, magnetic and biological characteristics. Such properties make them very effective in the removal of a huge range of pollutants including dyes pollutants.[38,39] So far, it was reported that the nanomaterials such as carbon nanotubes (CNTs) and graphene have good adsorption capacities toward pollutants in water.[40] Also, metal nanoparticles, and specifically zero-valent iron nanoparticles (nZVI) are considered among the primary metallic nanoparticles tested for the removal of water pollutants. This is attributed to a number of advantages which include easy preparation, high activity, low cost, and relatively lower toxicity. For such reasons, iron nanomaterials have been widely used for the removal of many types of dyes, including MO.[41,42,43]The material, however, suffers from rapid oxidation and high aggregation tendency. For this reason, other transition metals and bimetallic nanoparticles are being tested in comparison to iron, such as copper, which is applied in this study. Although the studies with zero-valent copper nanoparticles (nZVC) are still limited, copper and copper oxide surfaces can adsorb pollutants, or act as an electron donor in solution for some pollutants, leading to degradation of organic pollutants by electrochemical reactions.[44,45]

Methyl orange (MO) is one of the well-known acidic/anionic azo dyes which is chemically named (sodium dimethyl-amino-azo-benzene sulfonate) with chemical formula $Na{\cdot}C_{14}H_{14}N_3O_6S$.[46,47] The chemical structure of this dye is shown in scheme 1. Methyl orange has been widely used in many industrial sectors like textile, printing, paper, food and pharmaceutical industries.[48,49] In addition, it is used as an indicator in titration due to variation in its colour in acidic and basic mediums. When the medium is acidic it shows red color, but when it is basic, methyl orange appears in yellow color. [50] It has a bulk density of 1.28 g/cm^3, and its solubility in water is 5 g/L (at 20^{0}C). Its molecular weight is 327.34 g/mole.[51]

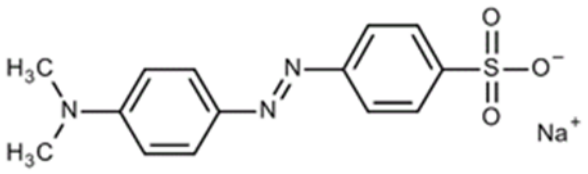

Scheme 1. Methyl orange structure

In an aqueous solution, MO molecule can be in different structures according to the protonic concentration, like the alkaline form (Figure 1.1 a). When the pH decreases, MO exists as a resonance hybrid between its quinine diimine (Figure 1.1 b) and azonium (Figure 1.1 c) structures. At equilibrium, a tautomeric structure of the MO molecule containing the ammonium group is also possible.[52] (Figure 1.1 d)

The two phenyls and one azo group (–N=N–) represent the chromophoric groups in methyl orange. Mainly two absorbance bands are observed, one of these bands occurs at nearly 465 nm due to a conjugated structure, formed by the azo bond under the strong influence of the electron-donating $(CH_3)_2N$ group. The other band appears at nearly 270 nm, and originates from a $\pi \rightarrow \pi^*$ transition related to aromatic rings.[45,53]

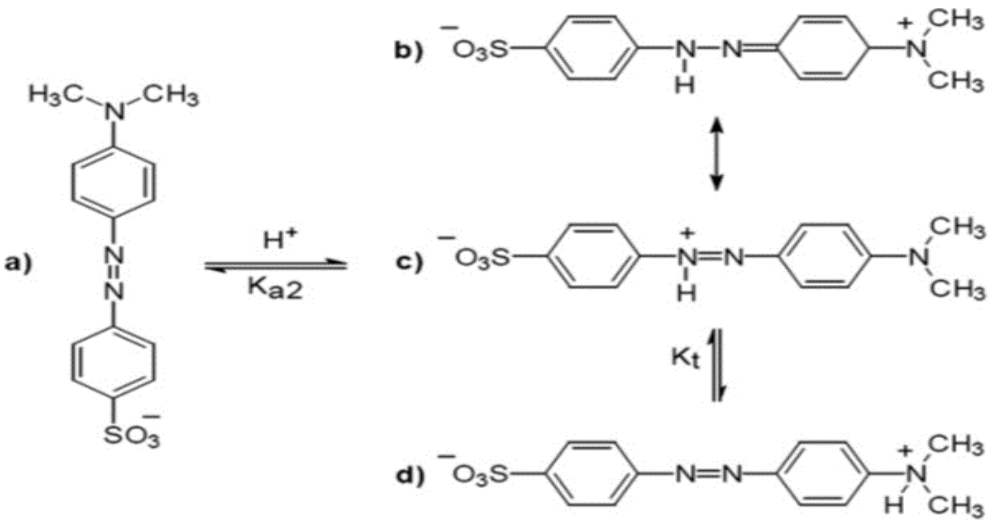

Figure[52] 1 .1: Alkaline form of MO (a), and its monoprotonated zwitterionic structures under acidic conditions: quinine diamine (b), the resonant form azonium (c), and the ammonium tautomer (d)

1.3 Nano Zero Valent Iron Particles (nZVI)

Iron (Fe) is one of the elements of Group (VIII) with atomic number 26. It is one of the most used and abundant metals on earth. The oxidation states of iron are +2, +3, +4, +6, and the most important among these are +2 and +3. It is naturally found as a mixture of stable isotopes: iron-56, iron-54, iron-57, and iron-58.[54,55] It can be extracted from rocks and minerals (iron ores), which are often rich in iron oxides. Also, it is usually found in the form of magnetite (Fe_3O_4), hematite (Fe_2O_3,), goethite (FeO(OH)), limonite ($FeO(OH)\cdot n(H_2O)$) or siderite ($FeCO_3$).[56]

Zero valent iron (ZVI) represents metallic iron. It is cheap and has no toxicity effect, and it has high reactivity, and can easily be oxidized. Iron oxides and oxyhydroxides (Fe_3O_4, Fe_2O_3, FeOOH, $Fe(OH)_2$, $Fe(OH)_3$, etc.) present on the surface of ZVI can contribute to the fixation of many organic and inorganic contaminants from water. So, it has been applied to treat water from different pollutants like volatile organic chlorides, metals and metalloid.[57,58,59] Zero-valent iron is a mild reducing reagent with a standard reduction potential $E^0 = -0.44$ V. So, in the existence of oxygen dissolved in water, organic pollutants can be oxidized by zero-valent iron. Firstly, oxygen reacts with ZVI and hydrogen peroxide is produced, as shown in equation (1). Then, water is produced from reduction of the H_2O_2 formed by ZVI, as shown in equation (2), or Fe^{2+} can react as a Fenton catalyst with H_2O_2 and produce hydroxyl radical, as shown

in equation (3). In this reaction, many organic pollutants can be degraded due to high reactivity of the formed radical.[60]

$$Fe^0 + O_2 + 2H^+ \rightarrow Fe^{2+} + H_2O_2 \qquad (1)$$

$$Fe^0 + H_2O_2 + 2H^+ \rightarrow Fe^{2+} + 2H_2O \qquad (2)$$

$$Fe^{2+} + H_2O_2 \rightarrow Fe^{3+} + \cdot OH + OH^- \qquad (3)$$

In the last decades, zero-valent iron nanoparticles have shown more efficiency toward removal/degradation of pollutants than macroscale ZVI.[60] Wang and Zhang were the first researchers who examined the use of nZVI for contaminated water treatment. After that this type of nanoparticle has been confirmed to possess high effectivity of removal of a wide range of common environmental contaminants such as chlorinated organic solvents, azo dyes, pharmaceutical products, metals, etc. The large surface area and unique chemical, catalytic, electronic, magnetic, mechanical and optical properties of nZVI have promoted their use in different applications, as compared to conventional iron. A number of possible removal pathways by nZVI have been suggested, including adsorption, co-precipitation, and surface mediated chemical reduction.[61]

Usually, there are two different approaches for nZVI synthesis; one is a top-down way in which the size of iron particles is reduced by milling, etching, and/or machining. The second way includes bottom-up methods in which the particles growth occurs by chemical reaction, positional and self-assembling mechanisms. In the bottom-up approach, the traditional way to synthesize nZVI is by chemical reduction of iron (III) or iron (II) by using sodium borohydride, as shown in following reactions.[62,63]

$$2Fe^{2+}_{(aq)} + 2BH_4{}^-_{(aq)} + 6H_2O_{(l)} \rightarrow 2Fe^0_{(S)} + 2B(OH)_{3(aq)+}7H_2$$

$$4\ Fe^{3+}_{(aq)} + 3\ BH_4{}^-_{(aq)} + 9\ H_2O_{(l)} \rightarrow 4\ Fe^0_{(s)} + 3\ H_2BO_3 + 12\ H_{2(g)}$$

This method was applied in this work, by using iron (III), and the details will be provided in the experimental section.

In some studies, green synthesis was developed and used. In that method, aqueous extracts obtained from some plants are used as reducing and capping agents. As an example, extracts of tea leaves, which contain polyphenols, was applied in nZVI synthesis process.[62]

1.4 Nano Zero-Valent Copper Particles (nZVC)

Copper is one of the transition metals which has an atomic number of 29, and has high thermal and electrical conductivity. It can be found in nature in a metallic form which is directly used (native metals), therefore it was used in ancient times in different regions. It is widely used in electrical wires, roofing and plumbing, and industrial machinery.[64,65] Since copper has a wide range of attainable oxidation states (Cu^0, Cu(I), Cu(II), and Cu(III)), it may undergo a variety of reactions.[66]

In the last decades, copper nanoparticles became a subject of interest to many researchers. Cu nanoparticles with inexpensive cost, wide availability, high electrical conductivity, small size, and large surface area are used in various applications, like in dental materials, water treatment, coating and manufacturing of lubrications, and conductive films.[67,68]

One of the most important biological properties is that Cu nanoparticles exhibit high antimicrobial activity against various types of microorganisms.[69] Therefore, this type of nanoparticles can be used as a disinfectant for wastewater.[67] In addition to the mentioned applications, Cu nanoparticles are widely used as a catalyst in various chemical reactions like hydrogen liberation and hydrocarbon oxidation. Also, it was reported to be used as a catalyst in the removal of some dyes from wastewater by reduction, such as the removal of Congo red (CR) dye from waste water.[70]

Different methods have been used to synthesize Cu nanoparticles. In top-down approaches, these nanoparticles can be synthesized by pulsed wire discharge, mechanical/ball milling, and solvothermal decomposition. On the other hand, Cu nanoparticles can be synthesized using bottom-up approaches through chemical reduction, electrochemical and sol-gel processes. In liquid-phase reduction a precursor of copper like copper salt is reduced to metallic copper by using many reducing agents like sodium borohydride, potassium borohydride, ascorbic acid and hydrazine.[71] This method was employed in this work using copper chloride dihydrate as a copper precursor, and sodium borohydride as a reducing agent, as shown in the following reaction.

$$CuCl_2.2H_2O_{(aq)} + 2NaBH_{4(aq)} \Rightarrow Cu^0_{(s)} + 2B(OH)_{3(aq)} + 2NaCl_{(aq)} + 3H_{2(g)}$$

Other methods with non-toxic solvents and environment-friendly materials, have been developed. It was reported that fish scale extracts, which acts as a stabilizing and reducing

agents, can be used to synthesize Cu nanoparticles, and the prepared NPs have been successfully used in the removal MB dyes from water. This synthesis method avoids the use of external reducing and stabilizing agents, templates, and solvents.[68]

1.5 Iron-Based Bimetallic Nanoparticles

Bimetallic nanoparticles represent a combination of two different metals in nano size. This combination can lead to new or improved chemical & physical characteristics, and can be utilized in different applications in various sectors like electronics, catalysis, and biomedicine. The properties of the obtained nanoparticles rely on their size, shape, composition, and architectures.[72,73] Bimetallic nanoparticles have four types of conceivable structures according to distribution ways of the two metal particles: core–shell NPs, subcluster NPs, alloy NPs, and multishell NPs (Figure 1.2).[74,75]

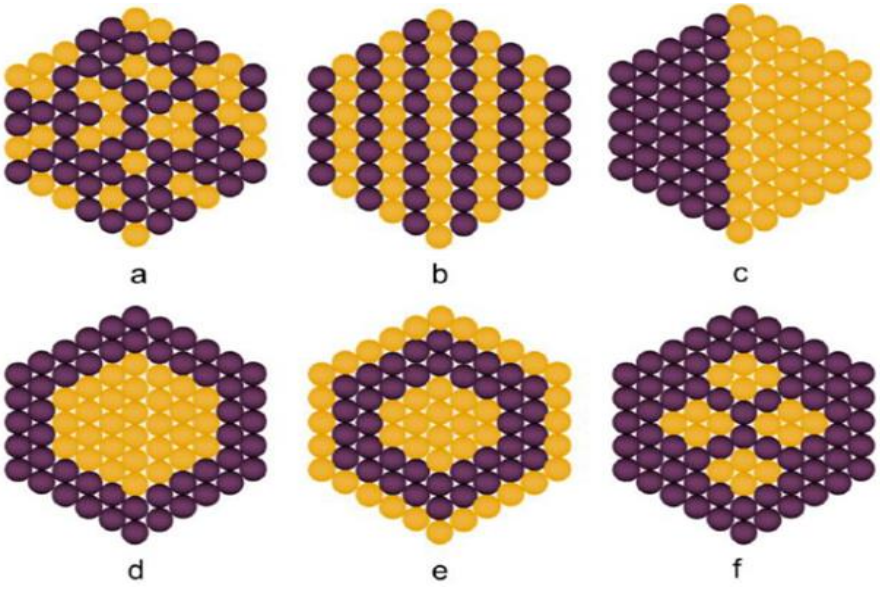

Figure 1.2: Types of bimetallic nanoparticles: (**a**) random alloyed, (**b**) ordered alloy, (**c**) subclusters (**d**) core-shell, (**e**) multi-shell core-shell, and (**f**) multiple core materials coated by a single shell material. Yellow and purple spheres represent two different kinds of metal atoms.[73]

In this system, the primary metal and secondary metal should be chosen according to their standard reduction potential (Table 1.1). The secondary metal is electropositive relative to the primary metal. In this system, the primary metal (like ZVI) acts as an electron donor while the secondary metal (like Pd, Ni and Cu) might behave like a catalyst. This metal is not consumed through the reaction, instead it may be rising the rate and efficiency of the reaction, and increasing the surface area and number of active sites on the primary metal (ZVI).[76]

Table 1.1: Standard electrode reduction potential values in aqueous solution at 25˚C. [76]

Metal	Half reaction	Standard electrode potential (E^0) V
Fe	$Fe^{2+} + 2e \Leftrightarrow Fe$	-0.440
Ni	$Ni^{2+} + 2e \Leftrightarrow Ni$	-0.257
Si	$SiO_2 + 4H^+ + 4e \Leftrightarrow Si + 2H_2O$	-0.909
Al	$Al^{3+} + 3e \Leftrightarrow Al$	-1.676
Zn	$Zn^{2+} + 2e \Leftrightarrow Zn$	-0.763
Mg	$Mg^{2+} + 2e \Leftrightarrow Mg$	-2.356
Pd	$Pd^{2+} + 2e \Leftrightarrow Pd$	0.915
Pt	$Pt^{2+} + 2e \Leftrightarrow Pt$	1.188
Cu	$Cu^{2+} + 2e \Leftrightarrow Cu$	0.340

Bimetallic nanoparticles can be synthesized by the following methods:[77]

Physical methods: such as laser irradiation, electrical method, and microwave irradiation These methods have some advantages over chemical methods, such as uniformity in the prepared nanoparticles. Furthermore, no solvent waste is generated. For example, in the laser irradiation method, bimetallic nanoparticles can be prepared using only high-intensity laser irradiation on an aqueous solution, with no need for chemical agents.[77]

Chemical methods: Reverse micelle, sol-gel, and co-precipitation methods are among them. These approaches have the advantages of being simple, affordable, and allowing for the synthesis of nanoparticles of various sizes and forms. Foreign atoms can also be doped during the synthesis process. [77] A solution of two metal precursors was added to a solution of precipitating agent, such as sodium hydroxide solution, utilizing co-precipitation procedures.

The particles grew and evolved into a spherical structure after being stirred properly. After that, deionized water should be used to wash the gelatinous product, and the pH should be adjusted until it is neutral. Finally, the gelatinous precipitate should be allowed to dry in the air to obtain a bimetallic powder. [78]

Biological methods: Environmentally friendly, quick, little industrial waste, and no harmful chemicals are among the advantages of biological methods over chemical and physical methods. Natural resources, such as plants and bacteria, can be used to synthesize nanoparticles in this process, which is known as 'green synthesis.' [77] Green tea extracts, for example, have been reported to be used as a reducing agent and a stabilizer in the synthesis of Fe-Cu nanoparticles with a size range of 60 to 120 nm. [73]

Iron-based bimetallic nanoparticles have attracted the attention of many researchers. It was reported that the combination between iron and other metals like Cu, Ni, and Pd, to obtain bimetallic nanoparticles can enhance and improve the adsorption rate when it is compared with mono iron nanoparticles. As a result, iron-based bimetallic nanoscale particles have been widely manufactured and utilized in different systems such as degradation of phenols, toxic metals, chlorinated organic compounds and dyes.[79]

Due to high reactivity, low cost, and non-toxicity of zero valent iron NPs, they are the most common metallic nanoparticles that were used for the removal of environmental pollutants.[61] But at the same time, iron NPs is highly sensitive to corrosion in aqueous solutions, through the electrochemical process shown in the following equations:

Under acidic condition:

$2\ Fe + 4\ H^{+}_{(aq)} + O_{2\ (aq)} \rightarrow 2\ Fe^{2+} + 2H_2O$ E = +1.67 V

$4\ Fe^{2+} + 4\ H^{+}_{(aq)} + O_{2\ (aq)} \rightarrow 4\ Fe^{3+} + 2H_2O$ E = + 0.46 V

Under neutral and alkaline condition:

$2\ Fe + 2H_2O \rightarrow 2Fe^{2+} + H_{2\ (g)} + 2OH^{-}$ E = -0.39 V

$2\ Fe^{2+} + 2H_2O \rightarrow 2Fe^{3+} + H_{2\ (g)} + 2OH^{-}$ E = -1.60 V

As a result, the reactivity of zero valent iron NPs toward the removal of pollutants will decrease. This is referred to as the coverage of the surface of zero valent iron NPs by iron hydroxides, which are formed during corrosion as shown in the following reaction:

$Fe^{3+} + 3OH^- \rightarrow Fe(OH)_3 \rightarrow FeOOH + H_2O$

In order to overcome these problems, a combination between iron and other metals, like Cu, to get bimetallic NPs have been performed.[80] In these iron-based bimetallic nanoparticles, Fe often behaves as an electron donor to reduce the pollutants according to their chemical potential, while the second metal, like Cu, is often inactive with a positive redox potential [$E(M^{n+}/M) > E(H^+/H_2)$] and acts as a catalyst to enhance the reactivity of iron.[76,80]

Bimetallic iron-based nanoparticles have been reported to be used for the removal of various types of environmental pollutants (as heavy metals, halogenated organic compounds, nitro and azo compounds, and oxyanions) through various proposed mechanisms. In cases with azo dyes pollutants, which have one or more azo (N=N) bonds, the N=N linkage dyes is responsible of dyes toxicity and carcinogenicity. It is reported that the bimetallic NPs of iron are very effective as catalysts in destroying the N=N bond during the reductive cleavage of the N=N bonds and oxidative degradation of the intermediate products.[80]

1.6 Literature Review

Different studies have been performed on methyl orange (MO) removal from water, including electrochemical degradation, advanced oxidation processes, coagulation-flocculation, and others. Adsorption is reported as one of the effective ways for removal of MO.[81]

Activated carbon is a common option for the adsorption of MO due to its special properties like porosity, stability, high surface area, and adsorption capacity.[82] Also, polymeric-based adsorbents like N-acyl thiolated chitosan were used for the adsorption of MO. It was reported that the percentage of the removal reached 88% and the maximum adsorption capacity was 588.2 mg/g.[83]

In addition, different types of nanoparticles were reported to result in important removal of this dye**.** Among these nanoparticles, iron and copper nanomaterials were used for adsorption of MO.[81] Animesh Debnatha and Krishna Deb et al., [84] prepared crystalline α-Fe_2O_3 nanoparticles and used it for adsorptive removal of MO from aqueous solution. They found that the removal process was effective with an adsorption capacity of 28.90 mg/g. The adsorption process was reported to follow second-order kinetic model.

In another study, CuO nanoflakes were synthesized and used for the adsorption of MO from an aqueous solution.[85] The removal of MO exceeded 90% at pH 2, and the thermodynamic analysis showed that the adsorbent process was spontaneous. The kinetic analysis indicated that the adsorption of MO followed pseudo-second-order kinetic model. In addition, the adsorption of MO on CuO was attributed to electrostatic attraction between the dye and adsorbent.

Nano zero-valent iron (nZVI) has widely used to treat water from various types of organic and inorganic pollutants.[86] It was found that nZVI has high efficiency towards MO removal. The results obeyed pseudo-second-order kinetic model. It was reported that the adsorption of MO on nZVI matchs Langmuir isotherm, which is reported to be indicative of monolayer adsorption.

In the decolorization of MO from aqueous solution by nZVI study, Jing Fan and Yanhui Guo et al.,[45] reported that the UV–vis spectra of MO before the adding of nZVI contains two absorbance bands, at 465 nm and 270 nm. After adding nZVI to the MO solution and starting the reaction, these two bands (465 & 270 nm) become weaker, and a band appeared at 248 nm. This was attributed to breaking the azo bond and formation of products. The band at 248 refers to sulfanilic acid, which is reported to be one of the products**.**

Due to the aggregation tendency of zero-valent iron (ZVI) nanoparticles which leads to reducing the reactivity of nZVI, bentonite-supported nZVI was synthesized for removal of MO from aqueous solutions.**[87]** The authors reported that the removal process was affected by different factors like pH, initial concentration of MO, dosage, and temperature. In addition, it was reported that the aggregation behaviour of nZVI decreased after using bentonite as a support material, and the reactivity increased. When B-nZVI was used, 79.46% of MO was removed, while only 40.03% of dye was removed when nZVI was then used.

Sunho Yoon and Sungjun Bae,[88] synthesized nZVI by a nother method, in which coal fly ash (CFA) was used as a source of Fe. The synthesized nZVI then used for the oxidative degradation of methyl orange by Fenton reaction. They reported that more than %96 decolorization of methyl orange was obtained by using the synthesized nZVI-CFA through Fenton reaction at pH 3.

In another study, Cu NPs were produced by using extract of Duranta Erecta fruit as a capping and reducing agent.[89] Then the synthesized NPs were used in the catalytic reduction of MO in the presence of $NaBH_4$ as a reducing agent. It was reported that Cu NPs exhibited

wonderful catalytic reduction for MO and obeyed the pseudo-first-order kinetics, with a rate constant of 8.6×10^{-3} s^{-1}.

In another study, the catalyst activity of nZVC loaded on filter paper-chitosan-titanium oxide heterogeneous support was tried for the removal of MO in the presence of $NaBH_4$.[90]

In addition to mono metallic NPs, different types of bimetallic NPs have been synthesized and studied for adsorption and degradation of organic pollutants.[91] Kgatle and Sikhwivhilu et al.,[92] discussed in their work the efficiency of Fe-Cu (5:1) bimetallic nanoparticles for MO degradation. It was reported that Fe-Cu (5:1) bimetallic NPs are more effective in the degradation of MO than nZVI. This is due to the synergetic effect between Fe and Cu which can improve the catalytic activity of the Fe/Cu system and also the degradation capabilities.

1.7 Purpose of the Study

So far various aspects of the application of nZVI in the removal of MO have been investigated. However, according to our literature survey, the application of Cu NPs or Fe-Cu NPs for MO removal was rarely studied previously. In particular, the effect of solution type on the removal process of MO using Fe^0, Cu^0 and Fe-Cu NPs remains one of the areas open to research, which was not addressed before for such systems.

Thus, this work study focuses first on the synthesis of Fe NPs, Cu NPs and Fe-Cu NPs, and then using the synthesized nano materials in the removal of MO from solutions with different solvents (W, W/E (1:1), W/DMSO (1:1)). The solutions, with various physical properties (Table 1.2)[93], were used to study the removal process, and the aggregation behavior and solvatochromic properties of MO were also investigated.

The prepared materials were characterized using Scanning Electron Microscopy (SEM) to investigate their nanoscale morphology. X-Ray powder Diffraction (XRD) was used to determine the mineralogical structure of the materials. X-Ray Photoelectron Spectroscopy (XPS) was employed to determine surface composition and the oxidation states of the surface species.

The dye concentration was monitored using UV-visible spectrophotometry. Experimental parameters such as the effect of time, effect of solvent type, temperature, and effect of NPs dose were investigated.

Table 1.2: Some physical properties of water, ethanol, and DMSO[93]

Solvent	**Normal Boiling point (°C)**	**Dipole Moment (Debye)**	**Dielectric Constant**	**Refractive Index**	**Surface Tension (mN/m)**
Water H_2O	100.0	1.82	80.1	1.345	72.0
Ethanol CH_3CH_2OH	78.4	1.69	24.5	1.361	22.0
DMSO $(CH_3)_2OS$	189.0	3.90	46.7	1.479	45.1

2. Experimental

2.1 Chemicals and Reagents

The following reagents were used without further purifications:

Methyl Orange, $C_{14}H_{14}N_3NaO_3S$.

Iron (III) chloride hexahydrate, $FeCl_3 \cdot 6H_2O$.

Copper (II) chloride dihydrate, $CuCl_2 \cdot 2H_2O$.

Sodium borohydride, $NaBH_4$.

Sodium chloride, NaCl.

Absolute ethanol (99.99%).

Milli-Q water.

0.1M HCl solution.

Hydrogen peroxide, H_2O_2, (10%).

All solutions were freshly prepared.

2.2 Calibration Curves of MO

Three different solvents were used to get three calibration curves for MO:

1. Water (W).
2. Water-Ethanol (W-E(1:1 v/v))
3. Water- Dimethylsulfoxide (W-DMSO (1:1 v/v))

1000 mg/L stock solutions of MO (Aldrich 140910) in three solvents W, W-E and W-DMSO were first prepared. Less concentrated solutions were then obtained by serial dilution using MQ water. To construct calibration curves for MO,the UV-visible spectra were obtained for the following concentrations: 10.0, 8.0, 4.0, 2.0 and 1.0 mg/L in each solvent, using UV-Vis spectrophotometer in the range of 200-700 nm.

2.3. Test of the Aggregation Behavior of MO

Two different dye concentrations were prepared; 8 and 10 mg/L MO in the following solvents:

1. Water (W).
2. Water/Ethanol (W-E (1:1 v/v)).
3. Water/ Dimethylsulfoxide (W-DMSO (1:1 v/v)).

The absorbance versus wavelength plots were used to determine the possible spectral shifts. Then maximum wavelength (λ_{max}) of MO in W, W-E (1:1) and in W-DMSO (1:1) was determined to calculate the transition energy of MO molecules in each of the three solutions.

2.4.1. Synthesis of Fe^0 NPs

Fe^0 NPs samples were synthesized by liquid reduction method, the Oxidation-reduction reaction can be written as:

$$4Fe^{+3} + 3BH_4^- + 9H_2O \rightarrow 4Fe^0{}_{(s)} + 3H_2BO_3^-{}_{(aq)} + 12H^+ + 6H_2$$

Fe^0 NPs were prepared by dissolving 7.24484g (26.8mmol) of $FeCl_3.6H_2O$ in 25.0 mL ethanol-water solution (4:1 v/v). The solution was kept under magnetic stirring for 15 min. In a separate container, 2.54g (67.2 mmol) of $NaBH_4$ was dissolved in 70.0 mL of water. The borohydride solution was then added quickly under continous magnetic stirring. The color of the iron solution changed to black and H_2 gas evolution was observed.

After the addition of borohydride solution, the mixture was kept under stirring for another 15 min, and vacum filtration was used to separate the produced Fe^0. The resulting Fe^0 NPs powder was washed three times with absolute ethanol, and dried at 60ºC for 3 hours.[94]

2.4.2. Synthesis of Cu NPS

Cu^0 NPs were prepared by dissolving 4.5688 g (26.8 mmol) of $CuCl_2.2H_2O$ in 25.0 mL ethanol-water solution (4:1 v/v). The solution was kept under magnetic stirring for 15 min. In a separate container 2.54 g (67.2 mmol) of $NaBH_4$ was dissolved in 70.0 mL of water. The borohydride solution was then added quickly under continous magnetic stirring. The color of the copper solution changed to black and H_2 gas evolution was observed.

After the addition of borohydride solution, the mixture was kept under stirring for another 15 min, and vacum filtration was used to separate the produced Cu^0. The resulting Cu^0 NPs powder was washed three times with absolute ethanol, and dried at 60ºC for 3 hours.[94]

The samples of Fe-Cu NPs at elemental mole ratio of 1:1 were prepared previously and used in this work.[100]

2.5. MO Removal Experiments

The final solutions obtained at the end of the removal experiments were diluted whenever needed before measuring the absorbance of MO solutions by UV-Vis spectrophotometry.

2.5.1. Effect of Solvent & NPs type on MO Removal

In this section, the removal process of MO in different solutions of W, W-E (1:1) and W-DMSO (1:1) was studied by using three types of NPs (Fe NPs, Cu NPs, and Fe-Cu NPs) at 298 K. The extent of the MO removal was investigated by introducing 0.025 g of NPs (Fe NPs , Cu NPs and Fe-Cu NPs) to 25 mL of 100 mg/L MO (in W , W-E and W-DMSO). Then the pH was measured, and the solutions were shaken at the selected temperature for four hours in a thermostated shaking water bath. Gravity filtration was then used to measure the absorbance of each solution and then the pH was measured.

2.5.2 Effect of temperature and NPs dose on the removal of MO in different solutions of W, W-E (1:1)

The effect of NPs (Fe NPs , Cu NPs, and Fe-Cu NPs) dose on the removal of MO in different solutions of W, W-E (1:1) at two different temperatures, 298 K and 323 K, was studied by introducing 0.005, 0.015, 0.025 and 0.035 g of NPs (Fe NPs , Cu NPs, and Fe-Cu NPs) to 25.0 mL of 100 mg/L MO (in W , W-E). Then the pH was measured, and the solutions were shaken once at 298 K and once at 323 K, for four hours in the thermostated shaking water bath. Gravity filtration was then used to measure the absorbance of each solution and then the pH was measured.

2.5.3 Salinity effect on MO removal

Four conentrations of NaCl (10, 20, 30 and 40 g/L) were used in MO solutions, by adding a suitable mass of NaCl into 25.0 ml of 100 mg/L MO solution containing 0.035g of NPs (Fe^0, Cu^0 and Fe-Cu). The solutions were kept in a thermostated shaking water bath at 298 K for four hours. Finally the solutions were filtered and the MO concentration was determined.

2.5.4. Removal of MO by Fenton-like process

Fe^0, Cu^0, and Fe-Cu NPs were used as Fenton-like catalysts in the removal of MO. The experiments were carried out in W and W-E solutions by introducing 0.050 g of NPs to 45.0 ml of 100 mg/L MO solution, and 5.0 ml of freshly prepared 10% (v/v) H_2O_2. 0.1 M HCl was used for pH adjustment of MO solutions before introducing the NPs (pH was approximately 3.37). Then the solutions were kept in a thermostated shaking water bath at 298 K for two hours.

2.5.5. MO removal kinetics

The effect of time on MO removal was studied at the initial MO concentration of 100.0 mg/L in two solvents, W and W-E (1:1), at two temperatures of 298 K and 323 K.
0.025 g samples of NPs were each introduced into 25.0 ml portions of MO solution, and the pH was measured for each solution. The mixtures were then shaken in a thermostated water bath for the contact times of 1 min, 15 min, 30 min, 1 hr, 2 hrs, 3 hrs, and 4 hrs. Gravity filtration was used to separate the liquid and the solid, then the absorbance of the solutions were measured using UV-Vis spectrophotometry.

2.6. Characterization

The characterization of the prepared NPs (Fe^0, Cu^0 and Fe-Cu), and the samples of MO solutions after removal process is described below.

The absorption spectra of the solutions were recorded using a single beam HP 8453 instrument that has an absorption range of 200-700 nm, and uses a photodiode array detector and deuterium lamp.

X-ray Photoelectron Spectroscopy (XPS) spectra were acquired using a PHI 5800 Multi Technique ESCA system with monochromatized A1-K_α (1486 eV) radiation at a take-off angle of 45, using pass energies at the analyzer of 29.35 EV for detail and survey scans, respectively.

Scanning Electron Microscopy (SEM) images of NPs were recorded using a Hitachi, S-5200 field-emission scanning electron microscope, Hitachi, Tokyo, Japan. The accelerating voltage is 10 kV , and the images were taken with the secondary electron detector. Moreover, EDX elemental spectra and mappings for selected elements of the nanoparticle materials where obtained.

Powder X-Ray Diffraction (XRD) data were collected on an STOE Stadi P diffractometer with Cu Kα1 (λ = 1.54 Å) source at 40 kV/ 40 mA. The samples were scanned from 2θ of 5 to 80 degree located at Helmholtz Institute Ulm, Germany.

3. Results and Discussion

3.1. Test of the Aggregation Behaviour of Methyl Orange (MO)

In the first part of this study, water, water-ethanol and water-DMSO solutions were used to test the removal of MO by Fe^0, Cu^0 and Fe-Cu NPs. The dye molecules can demonstrate different aggregation behavior in different solutions, and revealing this behavior is necessary to explain the results of the discoloration processes.

Classically, dye aggregates are categorized as H and J-type.[95] The dyes form aggregates through intermolecular forces such as hydrogen bonding and van der Waals force.[96] MO dye has a water-soluble group (usually sodium sulfonate), but at the same time it tends to aggregate by self-association of the hydrophobic parts of the molecular structure to form dimers, trimers, etc. One of the common ways used to study the aggregation process is UV-Vis absorption spectroscopy through comparing the positions of the absorption peak of the monomer and the aggregate peak.[95] It was reported that the formation of H-aggregates of dye molecules is marked by a spectral shift to the lower wavelength (blue shift) relative to the position of the absorption peak of the monomer. Also, as the solubility of the dyes in water increases, the aggregation chance decrease.[96]

In this work, the UV-Vis absorption spectra of MO dye in different types of solvents (water, water-ethanol, and water-DMSO) at MO concentrations of 10.0 mg/L and 8.0 mg/L was measured. The absorbance versus wavelength plots were used to determine the possible spectral shifts, as shown in Figure 3.1. The wavelength (λ_{max}) of MO in W, W-E(1:1) and in W-DMSO(1:1) solutions were determined, as shown in Table 3.1. In the three types of solvents, under the studied experimental conditions, no distinctive signs for dimers or higher order aggregates are seen in the spectra. However, a blue shift was observed in the case with MO in water-ethanol, and water-DMSO relative to the MO in water. No obvious intensity changes were observed in all cases.

It can be noted that the band shifts of the wavelengths is smaller for W-DMSO solution than W-E. The values of λ_{max} of the bands follow the order: W>W-DMSO>W-E, and this order is inversely proportional with the dielectric constant and surface tension values of the solvents (Table 1.2). Different solvents have different polarities, which inturn depends on a number of physical properties. It is reported that when the polarity increases, further stabilization of the excited state occurs compared to that of the ground state.[97]

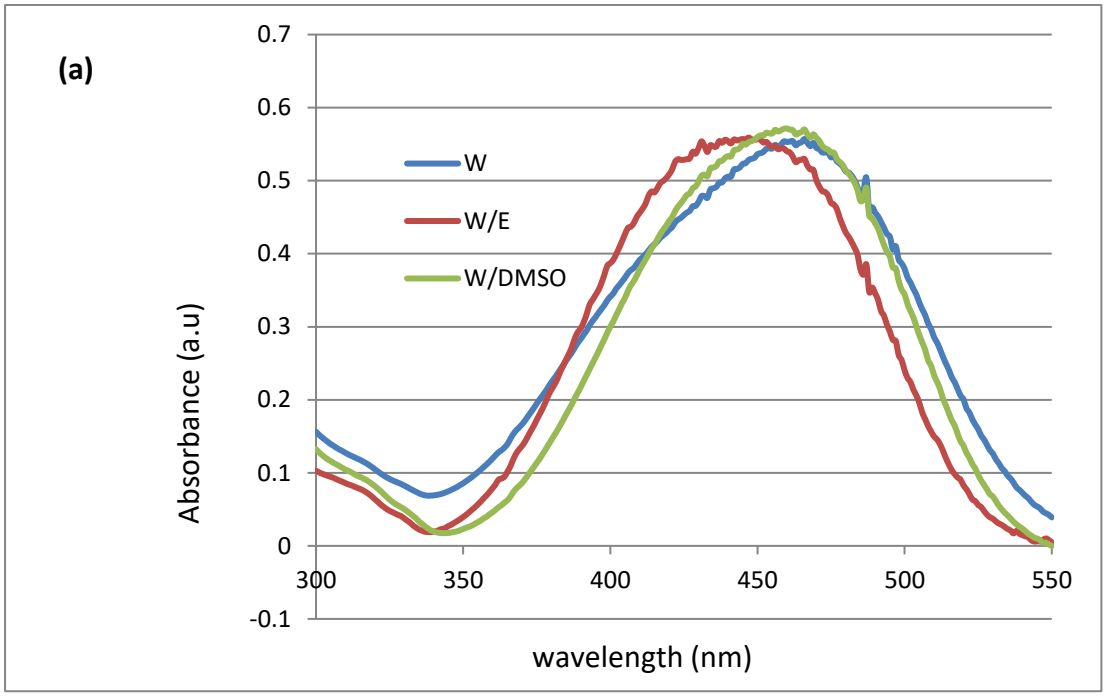

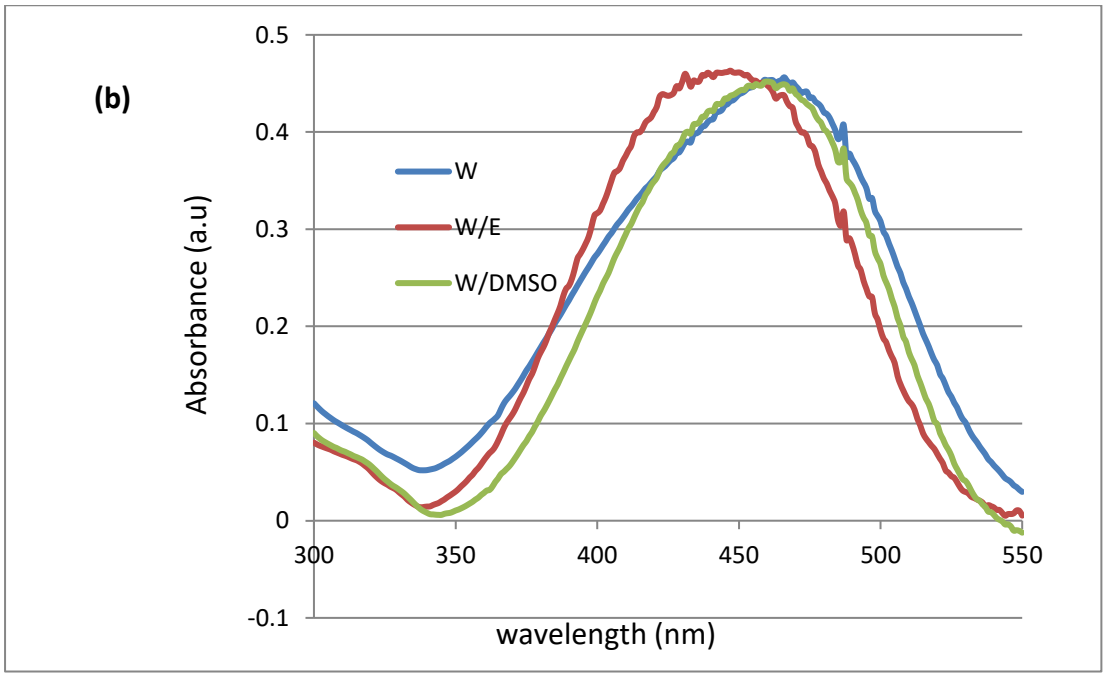

Figure 3 .1: Absorption spectra of MO in solvents W,W-E and W-DMSO at: **(a)** 10.0 mg/L, **(b)** 8.0 mg/L

Table 3. 1: Obtained values of λ_{max} of MO in W, W-E(1:1) and in W-DMSO(1:1)

Slovent type	λ_{max}
W	466
W-E	447
W-DMSO	460

The transition energy of MO molecules in each of the three solutions were calculated, as shown in Table 3.2, by using Rydbergs equation:[98]

$$E = N(hc/\lambda_{max}) \ldots\ldots\ldots\ldots\ldots\ldots\ldots\ldots (4)$$

Where;

E: Transition Energy(J/mol)

h: Plank's Constant ($6.626x10^{-34}$J.s)

c: Speed of light ($2.998x10^{8}$ m/s), λ: wavelenght (m)

N: Avogadro's number ($6.022x10^{23}$ mol^{-1})

Table 3. 2: The transition energy of MO molecules in each of the three solutions.

Solution type	Water	Water-Ethanol	Water-DMSO
λ_{max}	466	447	460
E (kJ/mol)	256.7	267.6	260.1

Apparently, as previously stated, as the values of dielectric constant and surface tension of the solvents increases, the values of λ_{max} increase and the values of E decrease. It is reported that higher wavelengths (or lower frequency) are observed for MO in aqueous solvents compared with organic solvents.[99]

The next sections will focus on the extent of removal of MO using Fe, Cu, Fe-Cu nanoparticles in different solvents under various experimental conditions.

3.2. Characterization of Fe NPs and Cu NPs

The nanoparticles samples of Fe and Cu prepared in this study were characterized by SEM, EDX, XRD and XPS techniques. Fe-Cu NPs used in this study were prepared earlier, and their characterization results were reported in a recent study.[100]

SEM images of Fe NPs (nZVI) are shown in Figure 3.2. The morphology of the material appears in its typical chain-like structure, which is attributed to the strong magnetic forces of among the individual Fe nanoparticles. This aggregation is reported to reduce the efficiency of the Fe NPs toward the removal of pollutants.[101]

The morphology of the prepared Cu^0 NPs was also examined by SEM. The copper nanoparticles exhibit nearly spherical shape, and since small Cu nanoparticles have a strong tendency to aggregate, some nanopatches, and something like Cu nanocluster were observed,[102] as shown in Figure 3.3.

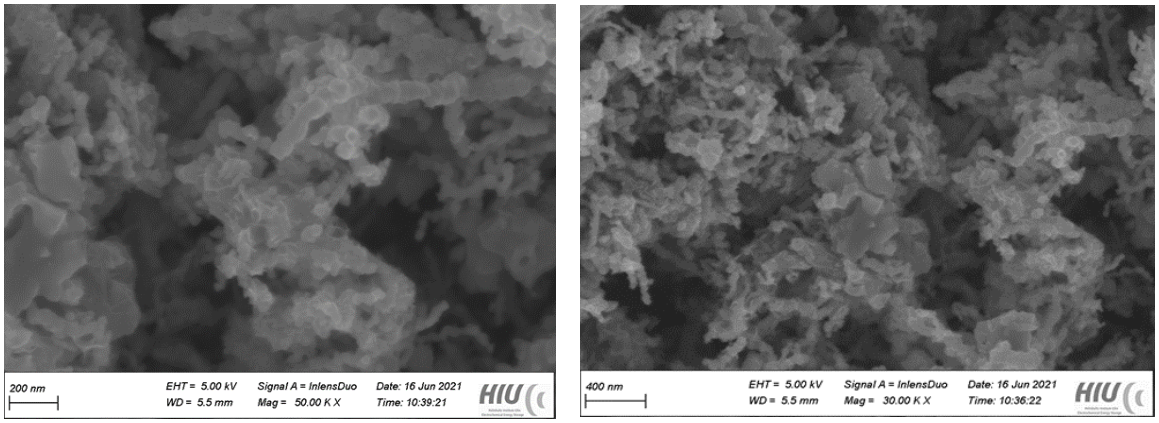

Figure 3 .2: Typical SEM images of Fe NPs at two different magnifications.

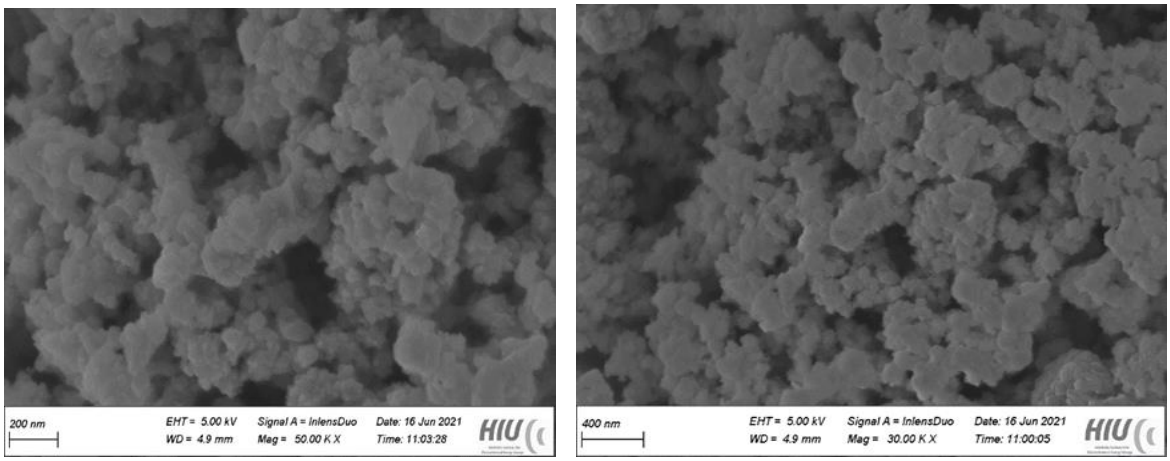

Figure 3. 3: Typical SEM images of Cu NPs at two different magnifications.

The EDX elemental spectra and mapping images of Fe NPs and Cu NPs are shown in Figures 3.4 and 3.5, respectively. As expected, the Fe samples are dominated by Fe and O, and the Cu samples are dominated by Cu and O. The oxygen content is not attributed totally to the samples, as some of the oxygen, and possibly carbon and nitrogen can arise from adventitious sources. The elemental mapping images shows that the O signals are intensively associated with Fe and Cu signals, possibly due to the presence of the oxide phases at the particles surface, which is in support of the core–shell model structure of these metallic nanoparticles.[103]

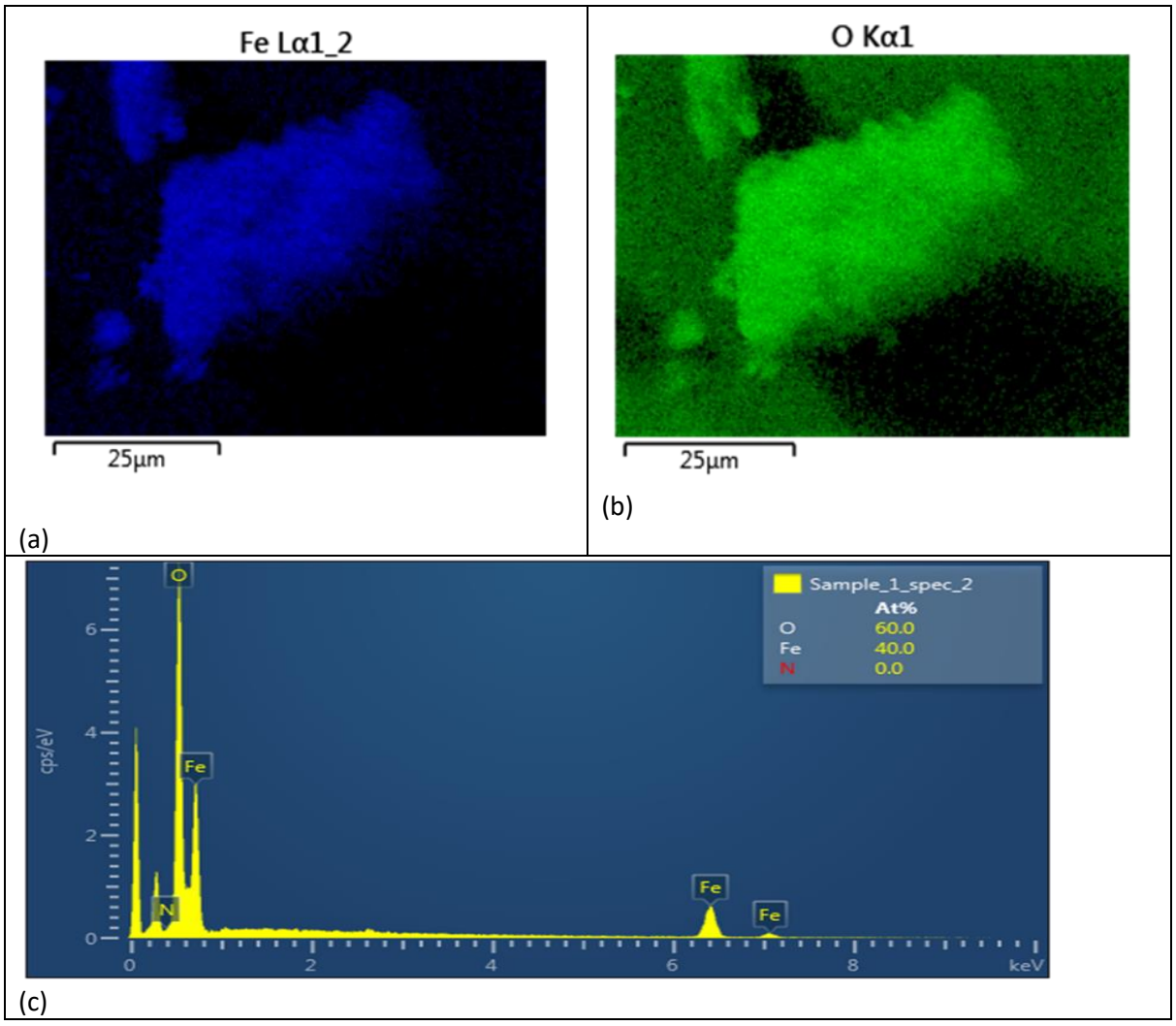

Figure 3. 4: Elemental mapping of (a) Fe signals (b) O signals, and (c) EDX spectrum of Fe NPs sample.

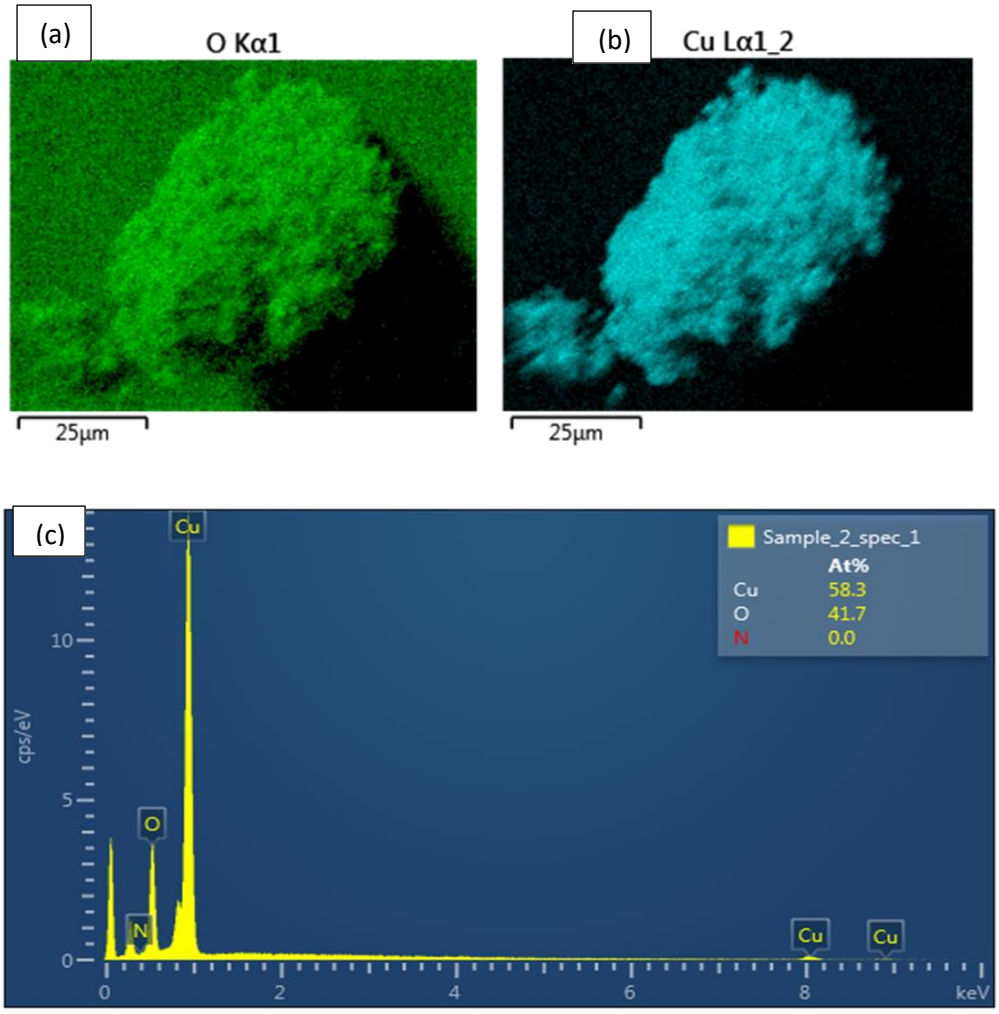

Figure 3. 5: Elemental mapping of (a) O signals (b) Cu signals, and (c) EDX spectrum, of Cu NPs sample.

The XPS spectrum of Fe 2p doublet obtained from Fe NPs is shown in Figure 3.6. The spectrum reveals a small shoulder at around 707 eV, suggesting the $2p_{3/2}$ peak of a zero-valent iron core (Fe^0) which confirms the presence of the metallic iron in the nanoparticle samples. The photoelectron peaks centered around 710 eV and 724 eV suggest that the shell was largely made up of iron oxides and iron oxyhydroxide. The peak deconvolution shows the presence of both of ferrous and ferric ions in the Fe sample. The features around 711 eV and 724 eV with difference of 13 eV originate from Fe^{2+} $2p_{3/2}$ and Fe^{2+} $2p_{1/2}$, respectively. While the features around 713 eV and 726 eV originate from Fe^{3+} $2p_{3/2}$ and Fe^{3+} $2p_{1/2}$, respectively. The appearance of the satellite feature indicates that iron ions are in high spin states, which is characteristic of certain iron compounds, like oxide compounds.[101,104,105]

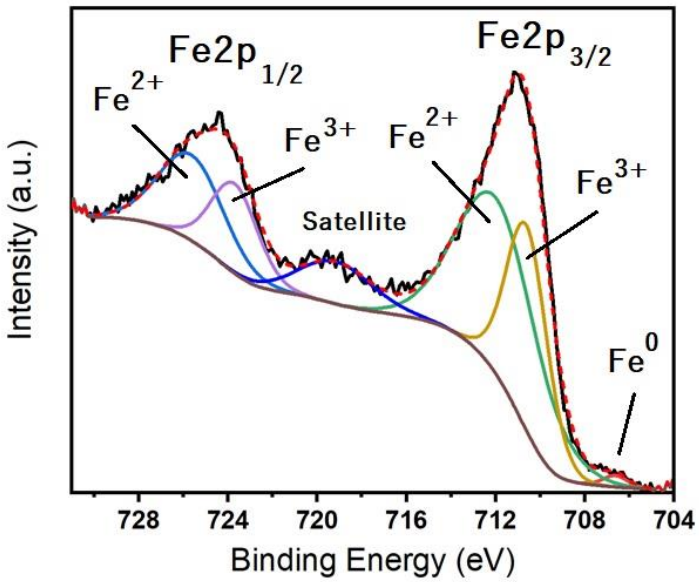

Figure 3. 6: XPS spectrum of Fe NPs showing the Fe2p doublet.

The XPS for a copper sample is shown in Figure 3.7. The peaks observed at 932.5 eV and 952.5 eV, with a difference of 20 eV, are assigned to Cu $2p_{3/2}$ and Cu $2p_{1/2}$ peaks, which can form envelopes for Cu(0), Cu(I) in Cu_2O, and Cu(II) in CuO. The presence of Cu(II) is also verified by the distinct shake-up satellite peaks in the spectrum. The Cu $2p_{3/2}$ satellite peak, which is nearly centered at about 944 eV in the Cu 2p XPS spectra may be associated with copper oxide.[106,107]

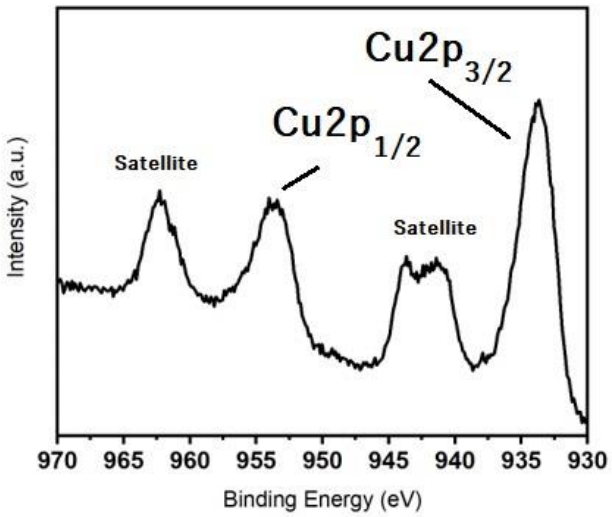

Figure 3. 7: XPS spectrum of Cu NPs showing the Cu2p doublet

The mineral phase and purity of the prepared iron and copper nanoparticles were examined using X-ray diffraction (XRD). The XRD pattern of Fe NPs is shown in Figure 3.8. The peak appearing at 2θ value of 44.7° matches with the characteristic (110) reflection of iron in its zero-valent state, Fe^0. The intensity of the reflection is low, indicating that the material is mostly amorphous.[108] Figure 3.9 shows the XRD pattern of Cu NPs. The reflection peaks at 2θ= 43.3, 50.4, 74.2 and 89.9 are reported to be indexed as (111), (200), (220) and (311) planes, respectively. The reflections match with metallic copper (face-centered cubic (fcc)). The sharp and strong peaks revealed that Cu nano-crystallites are highly oriented.[102]

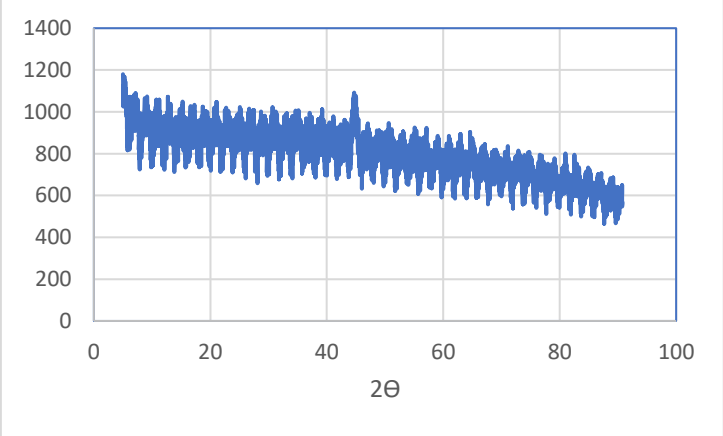

Figure 3. 8: XRD pattern of Fe NPs

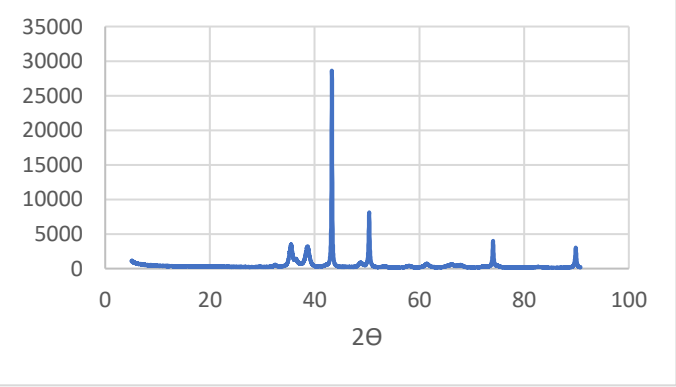

Figure 3. 9: XRD pattern of Cu NPs

3.3. Effect of Operation Parameters on MO Removal

Different parameters have been studied for the removal process of MO in different solutions. The effect of time was used to determine the kinetic parameters (rate constant, maximum capacity, and activation energy). The extent of MO removal was studied using the three types of NPs (Fe NPs , Cu NPs,and Fe-Cu NPs)**.** The effect of salinity, solvent type, type of nanoparticles, temperature, and nanoparticle doses on the removal process were studied and the results are shown in the following sections.

3.3.1. The effect of solvent and NPs type on MO removal

In this section, different types of solvents (W, W-E(1:1) and W-DMSO(1:1)) and different types of NPs (Fe^0, Cu^0 and Fe-Cu NPs) were used to study the effect of solvent type on the removal process of MO. The results, in terms of percentage MO removal, are shown in Figure 3.10.

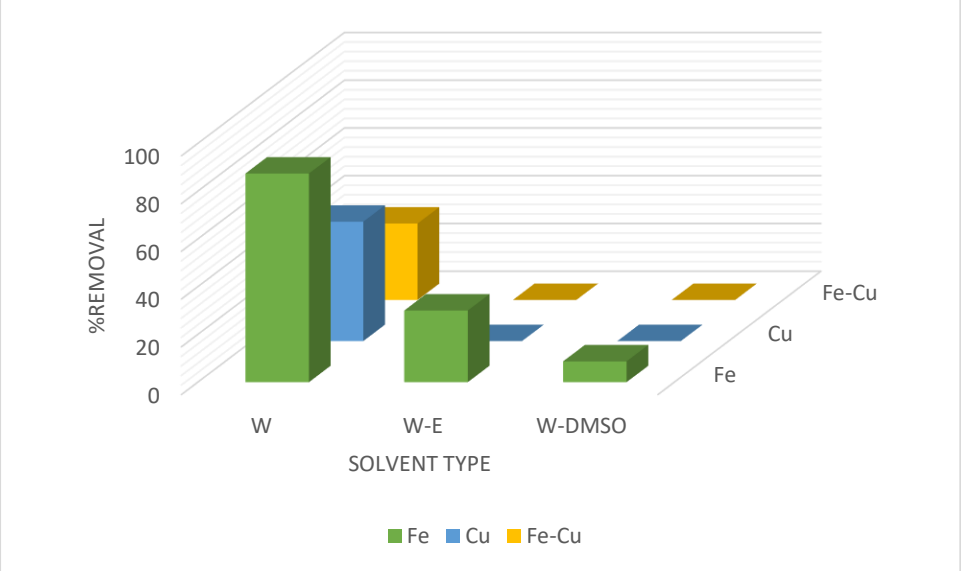

Figure 3.10: Percentage removal of MO in three types of solvents, with three types of nanoparticles.

The results showed that Fe^0 NPs are more effective in the removal of MO when compared with the other two types of nanoparticles. When Fe NPs are used, the trend of MO removal is: water > water-ethanol > water-DMSO. This trend is proportional with the trend of polarity of the

solvents. In the cases of Cu^0 and Fe-Cu NPs in water-ethanol and water-DMSO solvents, almost no dye removal was observed.

As shown in section 3.1, since the studies on the aggregation behavior of MO in the three solvents indicated no dimer or higher order aggregate formation, it can be concluded that the solute-solute interactions play minimal effects on the observed results. On the other hand, the solute-solvent interactions seem to directly affect the extent of MO removal in the three different solvents. Like MO molecules, ethanol and DMSO molecules consist of hydrophobic and hydrophilic parts. So solute-solvent interactions in water-ethanol and water-DMSO solutions compared with water solutions could be causing smaller extents of removal. Moreover, the molecules of ethanol and DMSO in the two mixed solvents might be forming solvation spheres around the nanoparticles in which the hydrophilic part is directed towards the nanoparticle surface, while the hydrophobic part extends to other side into solution, possibly causing a steric hindrance acting against the accessibility of the dye molecules to the nanoparticle materials.

The following sections discuss the MO removal under different conditions. Due to the poorer performance of the water-DMSO solvent, the coming experiments were performed on a comparative basis between pure water and water-ethanol solvents.

3.3.2. Effect of NPs dose

In order to study the effect of nanoparticle dose on the removal process, 0.005, 0.015, 0.025 and 0.035 g samples of NPs (Fe^0 NPs, Cu^0 NPs,and Fe-Cu NPs) was introduced into 25 mL of 100 mg/L MO in W and W-E solvents. The temperature was kept at 298 K in these experiments. The results, in terms of percentage MO removal are shown in Figure 3.11.

The results clearly show that water solutions lead to better removal of MO over binary solutions containing water and ethanol. Also, in cases with water solutions for the three types of nanoparticles used in these experiments, the removal of MO increases with an increase in the NPs dose. This could be due to the fact that the availability of surface-active sites increases with the increased dose of adsorbent.[109]

In addition, the results indicate that Fe^0 nanoparticles are more effective in MO removal than Cu and Fe-Cu nanoparticles under all conditions, and it is possible to attain almost a complete removal of MO from water at the highest nanoparticle dose used in these experiments.

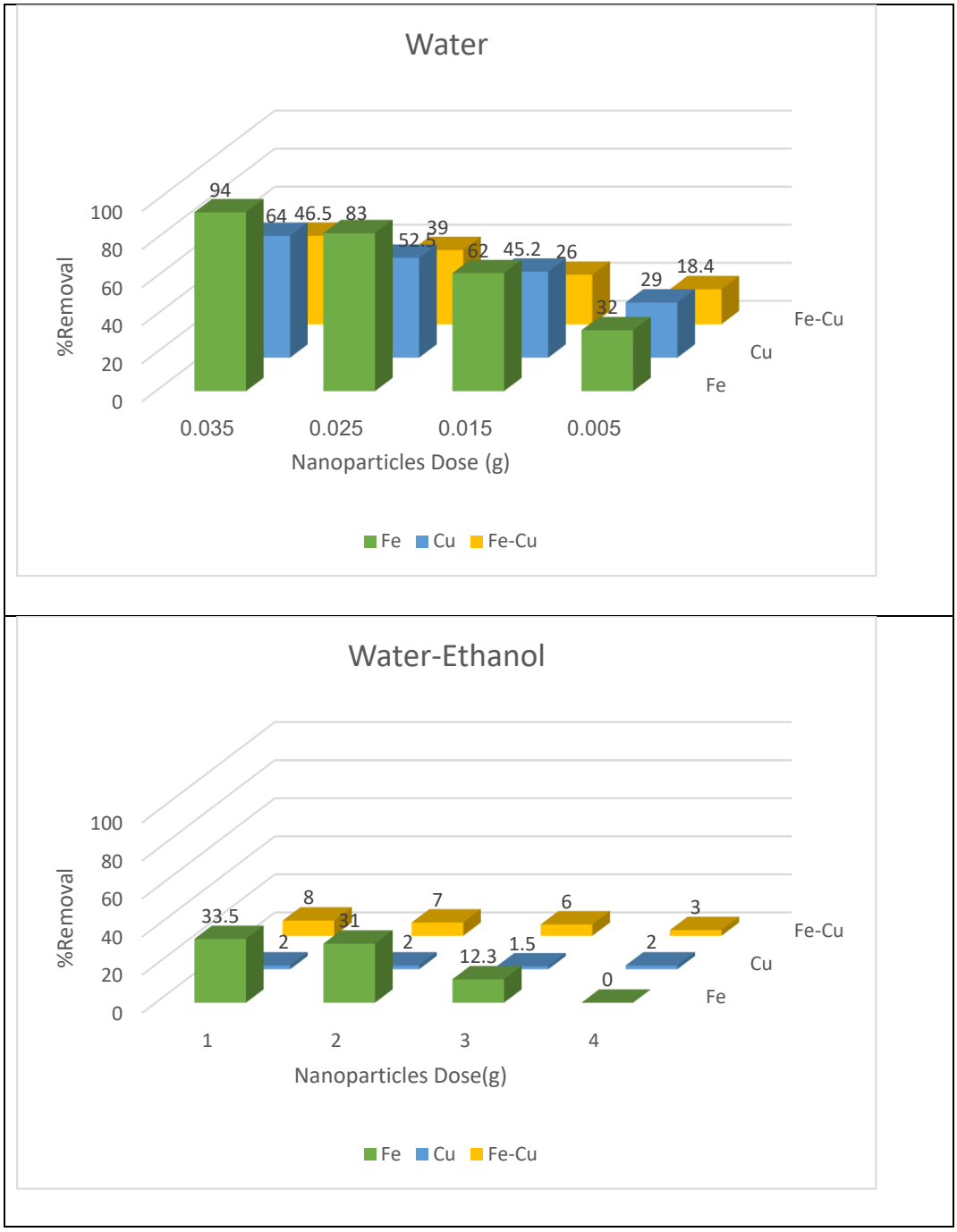

Figure 3.11: Variation of the percentage removal of MO in water and water-ethanol solutions, using Fe, Cu, and Fe-Cu nanoparticles at 298 K.

Langmuir, Freundlich, Tempkin, Dubinin-Radushkevich, and Harkins-Jura isotherms were used to fit the experimental data. The coefficient of determination (R^2) of the linear fits of the isotherms is given in Table 3.3.

The nonlinear equations of these isotherms are:

Langmuir model: $Q = \frac{Q_m K_L C}{1+K_L C} \ldots\ldots\ldots\ldots\ldots\ldots\ldots (5)$

Freundlich model: $Q = k_F C^{1/n} \ldots\ldots\ldots\ldots\ldots\ldots\ldots (6)$

Temkin model: $Q = B_T \ln(A_T C) \ldots\ldots\ldots\ldots\ldots\ldots (7)$

Dubinin – Radushkevich model:

$Q = Q_m e^{-K\varepsilon^2}$ $in\ which\ \varepsilon = RT \ln\left(1 + \frac{1}{C}\right) \ldots\ldots\ldots (8)$

Harkins-Jura: $Q = \sqrt{\frac{\beta}{logC - \alpha}} \ldots\ldots\ldots\ldots\ldots\ldots\ldots\ldots (9)$

In all equations, Q stands for equilibrium dye concentration on the solid phase (mg/g), and C is the equilibrium liquid concentration (mg/L). the other terms in equations stands for the isotherm constants.[110]

According to the linear regression results, poor correlations were obtained for Langmuir, Dubinin-Radushkevich, and Temkin isotherms. On the other hand, Harkins-Jura isotherm provided the best correlation followed by Freundlich isotherm. The linear fits obtained using these two models are shown in Figure 3.12 (a,b). Harkin-Jura (H-J) isotherm model supposes the possibility of multilayer adsorption on the surface of adsorbent having a heterogeneous pore distribution.[109]

Freundlich isotherm is usable to adsorption processes that happen on heterogonous surfaces. This isotherm affords an expression which realizes the surface heterogeneity and the exponential distribution of active sites and their energies. The linear form of the Freundlich isotherm is as follows:

$\ln Q_e = \ln K_F + 1/n \ln C_e$ ……..(10)

Where K_F is the adsorption capacity (L/mg) and $1/n$ is referred to as the adsorption intensity; it also indicates the relative distribution of the energy and the heterogeneity of the adsorbate sites.[110]

The values of K_F and 1/n in Freundlich isotherm model were determined when Fe^0, Cu^0 and Fe-Cu NPs were used for the removal processes performed with water solvent and the results are shown in Table 3.4. The MO adsorption onto Fe^0 is considered to be favorable because the values of 1/n are less than 1, and n in the range 2–10. In general, when the value of 1/n is less than 1 and the value of n in the range of 2–10 indicates good, 1–2 moderately difficult and below 1 poor adsorption (as in case with Cu^0 & Fe-Cu) characteristics.[109]

Table 3.3: The obtained R^2 values from isotherm models

Fe^0				
Isotherm	R^2 (W at 298K)	R^2 (W-E at 298K)	R^2 (W at 323 K)	R^2 (W-E at 323 K)
Langmuir 1	0.901	0.181	0.997	0.734
Langmuir 2	0.802	0.311	0.977	0.077
Langmuir 3	0.567	0.968	0.927	0.181
Langmuir 4	0.567	0.968	0.927	0.181
Freundlich	0.909	0.672	0.968	0.037
Tempkin	0.829	0.760	0.994	0.023
D-R	0.562	0.595	0.882	0.079
Harkins-Jura	0.996	0.150	0.748	0.069
Cu^0				
Isotherm	R^2 (W at 298 K)	R^2 (W-E at 298K)	R^2 (W at 323 K)	
Langmuir 1	0.708	0.003	0.583	
Langmuir 2	0.902	0.004	0.665	
Langmuir 3	0.960	1.000	0.998	
Langmuir 4	0.960	1.000	0.998	
Freundlich	0.898	0.013	0.619	

Tempkin	0.822	0.059	0.576	
D-R	0.748	0.013	0.602	
Harkins-Jura	0.964	0.050	0.732	
Fe-Cu				
Isotherm	R^2 (W at 298K)	R^2 (W/E at 298K)	R^2 (Wat 323 K)	R^2 (W/Eat 323 K)
Langmuir 1	0.396	0.833	0.599	0.626
Langmuir 2	0.784	0.849	0.983	0.925
Langmuir 3	0.949	0.999	0.148	0.880
Langmuir 4	0.949	0.999	0.148	0.880
Freundlich	0.728	0.899	0.988	0.918
Tempkin	0.654	0.938	0.974	0.892
D-R	0.665	0.903	0.943	0.963
Harkins-Jura	0.871	0.787	0.906	0.877

Table 3.4: Freundlich isotherm constants.

NPs	K_F	1/n	N
Fe^0	35.4	0.33	3.1
Cu^0	0.056	1.82	0.55
Fe-Cu	0.011	2.0	0.50

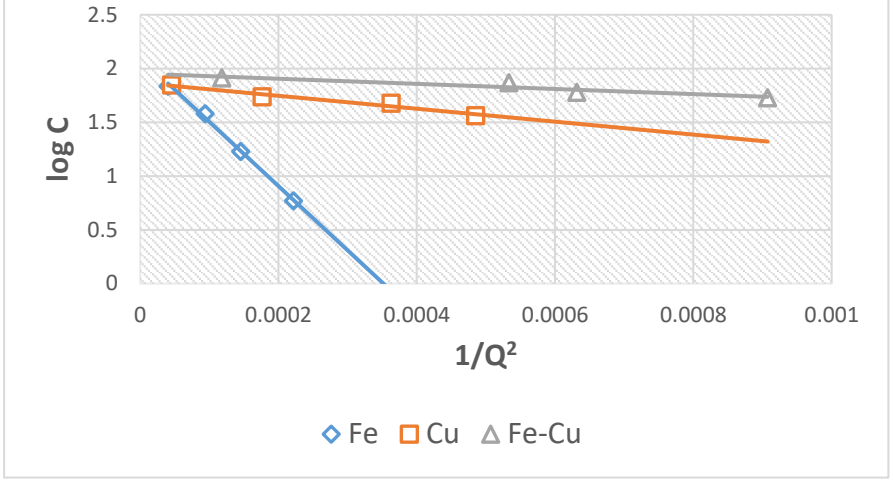

(a)

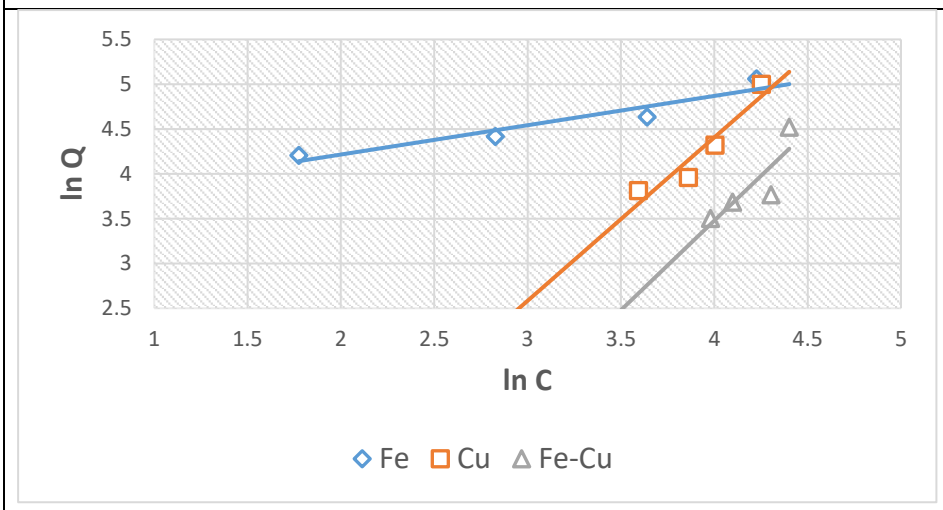

(b)

Figure 3.12: (a,b). The linear fits of MO data in water solutions obtained using: (a) Harkins-Jura isotherm, and (b) Freundlich isotherm models.

3.3.3. Effect of Temperature

The experiments performed to study the effect of NPs dose at 298 K were repeated at 323 K. The results, in terms of percentage MO removal are shown in Figure 3.13 (a,b). In agreement with the previous results, water solutions were much better than W-E solutions for the removal of MO. In the case of using Fe^0 and Fe-Cu NPs, increasing the temperature resulted in increasing the removal of MO in both solutions of W and W-E, and as a result the adsorption capacity (Q) increases. It has been reported that temperature has two main effects on the adsorption process. It is known that an increase in temperature increases the mobility of the

adsorbate molecules in the solution, and the rate of diffusion of these molecules toward the adsorbent particles, as a result of the decreased viscosity of the solution. Therefore, it can be concluded that the adsorption of MO onto Fe^0 and Fe-Cu NPs is an endothermic process.[111]

In contrast, when using Cu^0 NPs, increasing the temperature results in a decrease in the percentage removal and adsorption capacity. This can be explained by the exothermic spontaneity of the adsorption process and by the weakening of bonds between MO molecules and active sites of adsorbents at high temperatures.[112]

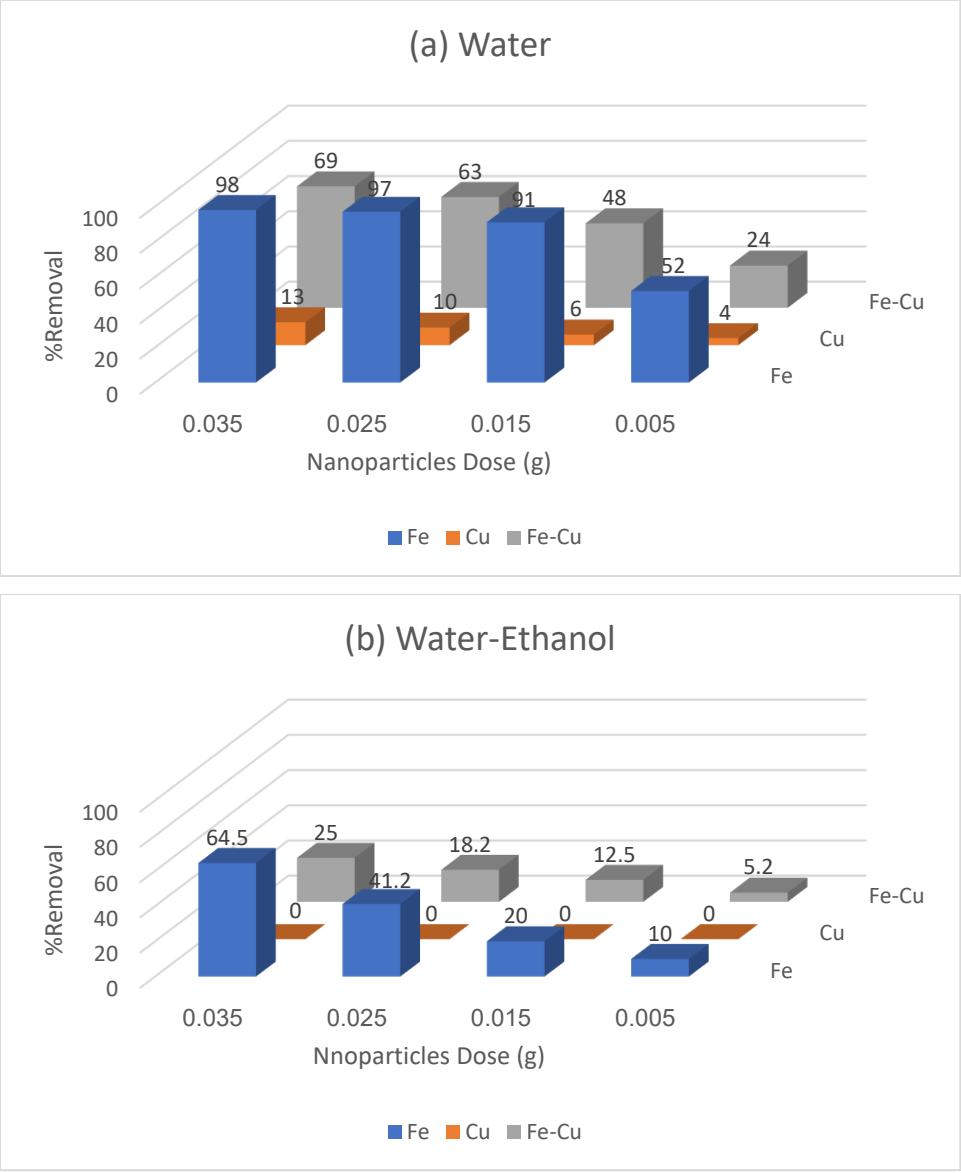

Figure 3.13: Variation of the percentage removal of MO in (a) water and (b) water-ethanol solutions, using Fe, Cu, and Fe-Cu nanoparticles at 323 K.

Langmiur, Freundlich, Tempkin, Dubinin-Radushkevich and Harkins-Jura isotherms were used to fit the data. The coefficient of determination (R^2) of the linear fits of the isotherms is given in Table 3.3. In the case of Fe^0 NPs for the removal process of MO in water, according to the linear regression results, poor correlations were obtained for Freundlich, Dubinin-Radushkevich and Harkins-Jura isotherms. On the other hand, Langmuir type 1 isotherm provided the best correlation followed by Tempkin isotherm. The linear fits obtained using this type are shown in Figure 3.14.

Langmuir adsorption isotherm was initially derived to describe the gas-solid system, but was then extended to liquid-solid systems. This isotherm suggests that adsorption is proportional to the fraction of the surface of the adsorbent that is open while desorption is proportional to the fraction of the adsorbent surface that is covered .[110]

The Langmuir isotherm is valid for monolayer adsorption onto a surface with a finite number of identical sites. In this case, MO adsorption conforms to the Langmuir model, the adsorption process expressed as:

$C_e / Q_e = 1/(K_L . Q_m) + C_e / Q_m$ ……(11)

Where Q_m (mg/g) is the maximum adsorption capacity and K_L (L/mg) is the Langmuir constant related to the adsorption equilibrium. The essential characteristics of the Langmuir isotherm can be expressed by means of 'R_L' a dimensionless constant referred to as the separation factor or equilibrium parameter. The R_L is defined as:

$R_L = 1/ (1+K_L . C_0)$ ……..(12)

R_L values indicate the adsorption to be unfavorable when $R_L > 1$, linear when $R_L = 1$, favorable when $0 < R_L < 1$, and irreversible when $R_L = 0$.[111]

The R_L value for this case calculated from Langmuir linear equation resulted from plot C/Q vs C :

$$\frac{C_e}{Q_e} = 0.0034 C_e + 0.0235$$

The slope = $1/Q_m = 0.0034$, intercept=$1/(K_L.Q_m) = 0.0235$

so; $Q_m = 294.1$ mg/g , $K_L = 0.145$ L/mg

Thus; $R_L = 0.065$ indicates that the adsorption of MO onto Fe^0 at 323K is favorable.

In this study, Langmuir equations in 4 different types of linear expressions have been used to find the best linear type based on the experiment of methyl orange adsorption from its water solution onto NPs.

The linear form of Langmuir equation originated from Eq. 5 is expressed as:

$$\frac{C_e}{Q_e} = \frac{1}{K_L Q_m} + \frac{C_e}{Q_m} \qquad Type\ 1 \dots\dots\dots\dots\dots (11)$$

The rearrangement of This equation results in obtained another 3 different linearized types of Langmuir expressions:[113]

$$\frac{1}{Q_e} = \frac{1}{K_L Q_m}\frac{1}{C_e} + \frac{1}{Q_m} \qquad Type\ 2 \dots\dots\dots\dots\dots (13)$$

$$Q_e = \frac{-Q_e}{K_L C_e} + Q_m \qquad Type\ 3 \dots\dots\dots\dots\dots\dots (14)$$

$$\frac{Q_e}{C_e} = -K_L Q_e + K_L Q_m \qquad Type\ 4 \dots\dots\dots\dots\dots (15)$$

In the case of using Cu^0 and Fe-Cu NPs for MO removal process from water at 323 K, according to the linear regression results, poor correlations were obtained for Freundlich, Dubinin-Radushkevich and Harkins-Jura, Tempkin isotherms. On the other hand, Langmuir type 3 and 4 isotherms provided the best correlation in case with Cu^0. For Fe-Cu Langmuir type 2 was the best, as shown in the Table 3.3. In this case, R^2 values obtained from the four linear expressions of Langmuir equations were largely different. It was noted that expression of type 3 and type 4 had the R^2 value higher than R^2 value of type 1 and type 2 for the MO adsorption on Cu^0. Also, the R^2 values of type 2 expressions are higher than R^2 values of type1, type3 and type4 expression for the MO adsorption on Fe-Cu. These results indicated that different linear forms of the same Langmuir isotherm equations significantly will affect calculations of the parameters. These divergent outcomes show the real complexities and problems in estimating the isotherm parameters by the linearized method. The different outcomes for different linearization form of Langmuir isotherm equations were produced by the variation in the error structure that would get varied upon the linearizing technique of the nonlinear equation.[113]

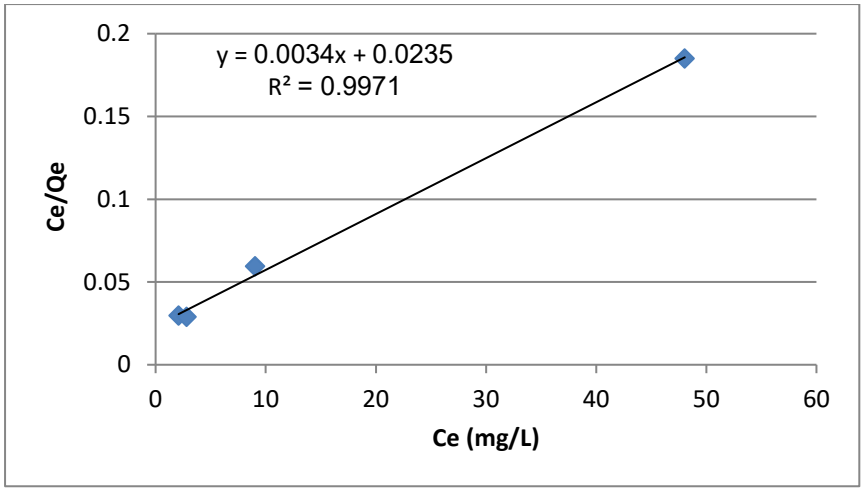

Figure 3. 14: The linear fits of MO data in water solutions at 323 K using Fe^0 NPs obtained with using Langmuir type1 isotherm.

The results obtained from the effect of temperature were used to calculate the thermodynamic parameters of sorption; Gibbs free energy changes and enthalpy changes. Standard Gibbs free energy change can be calculated using the well-non thermodynamic relation:[114]

$\Delta G^0 = -RTlnK$ ……(16)

Where R is the universal gas constant, 8.314 J/mol K; T is the absolute solution temperature, and K representing the thermodynamic equilibrium constant.

To evaluate values of K 'equilibrium constant' of sorption, the distribution ratio (or distribution coefficient), R_d or K_d can be used. The R_d (or K_d) is defined as the ratio of concentration of the sorbate on the solid to its concentration in the liquid (Q_e/C_e).

Thus, $R_d = Q_e/C_e$ ……..(17)

And the equilibrium constant (K) can be obtained by multiplying the R_d value with the mass of the sorbent, in g, and dividing it by the solution volume in L.[114]

So, $K = R_d . M/V$ …….(18)

The results of Gibbs free energy for removal of MO by using Fe^0, Cu^0 and Fe-Cu NPs in two solvents at 298 K and 323 K are shown in Tables 3.5, 3.6 and 3.7.

Table 3.5: Gibbs free energy for removal of MO by using Fe^0 NPs in two solvents at 298 and 323 K

Fe^0	W, at 298K		
NPs dose(g)	R_d	K	ΔG° (kJ/mol)
0.035	11.44	16.02	-6.87
0.025	4.91	4.91	-3.94
0.015	2.71	1.62	-1.20
0.005	2.30	0.46	1.93
Fe^0	W, at 323K		
0.035	33.54	46.96	-10.34
0.025	34.50	34.50	-9.50
0.015	16.80	10.07	-6.20
0.005	5.40	1.08	-0.21
Fe^0	W-E, at 298K		
0.035	0.40	0.50	1.70
0.025	0.45	0.45	1.97
0.015	0.23	0.14	4.90
0.005	0	0	-
Fe^0	W-E, at 323K		
0.035	1.30	1.82	-1.60
0.025	0.70	0.70	0.95
0.015	0.44	0.25	3.72
0.005	0.56	0.11	5.90

Table 3. 6: Gibbs free energy for removal of MO by using Cu^0 NPs in two solvents at 298 and 323 K

Cu^0	W, at 298K		
NPs dose(g)	R_d	K	ΔG^0 (kJ/mol)
0.035	1.25	1.75	-1.40
0.025	1.10	1.10	-0.250
0.015	1.40	0.825	0.480
0.005	2.11	0.422	2.13

Cu^0	W, at 323K		
0.035	0.10	0.146	5.20
0.025	0.11	0.111	5.90
0.015	0.11	0.066	7.30
0.005	0.22	0.045	8.32
Cu^0	W-E, at 298K		
0.035	0.014	0.020	9.64
0.025	0.020	0.020	9.64
0.015	0.025	0.015	10.40
0.005	0.102	0.020	9.64

Table 3.7: Gibbs free energy for removal of MO by using Fe-–Cu NPs in two solvents at 298 and 323 K

Fe-Cu	W, at 298K		
NPs dose (g)	R_d	K	ΔG^0 (kJ/mol)
0.035	0.62	0.87	0.35
0.025	0.66	0.66	1.02
0.015	0.60	0.35	2.60
0.005	1.13	0.22	3.70
Fe-Cu	W, at 323K		
0.035	1.60	2.20	-2.11
0.025	1.70	1.70	-1.41
0.015	1.52	0.910	0.252
0.005	1.55	0.310	3.140
Fe-Cu	W-E, at 298K		
0.035	0.064	0.089	5.98
0.025	0.074	0.074	6.45
0.015	0.112	0.067	6.70
0.005	0.154	0.030	8.61
Fe-Cu	W-E, at 323K		
0.035	0.240	0.334	2.94
0.025	0.232	0.232	3.91

0.015	0.239	0.143	5.22
0.005	0.274	0.055	7.80

As can be seen from the tables above, the K values for MO in water solutions are clearly larger than those in water-ethanol solutions.

In the case of using Fe^0 NPs for the removal of MO from water at 298 and 323K, the ΔG^o negative values indicate that the MO adsorption reaction onto Fe NPs favors the products over the reactants. This is true for any case leading to negative values of ΔG^o, since K values would then be greater than one. On the other hand, in all cases, positive values ΔG^o result from limited MO sorption, which leads to K values less than one.

The K values obtained at the two temperatures were used to calculate the enthalpy changes (ΔH^0) associated with the uptake of MO from the two solutions (W, W-E) at 4 NPs doses. For this purpose, Van't Hoff equation was used;[115]

$$ln\frac{K_2}{K_1} = \frac{\Delta H^o}{R}\left(\frac{1}{T_1} - \frac{1}{T_2}\right) \dots\dots\dots\dots\dots (19)$$

Where K_1 and K_2 are the equilibrium constants of the reaction at two different temperatures; T_1 and T_2 respectively. The obtained values are given in Tables 3.8, 3.9 and 3.10.

Table 3.8: The values of ΔH^0 associated with removal of MO from the two solutions (W, W-E) at 4 Fe^0 NPs doses at two temperatures (298,323K)

Fe^0 dose (g)	K_1 at 298 K	K_2 at 323 K	ΔH° (kJ/mol)
	Water		
0.035	16.02	46.96	34.42
0.025	4.90	34.46	62.40
0.015	1.62	10.07	58.40
0.005	0.46	1.08	27.40
	W-E		
Fe^0 dose (g)	K_1 at 298 K	K_2 at 323K	ΔH° (kJ/mol)
0.035	0.51	1.82	40.89
0.025	0.45	0.700	14.076
0.015	0.14	0.250	18.54
0.005	0	0.112	-

Table 3.9: The values of ΔH^0 associated with removal of MO from water at 4 Cu^0 NPs doses at two temperatures (298, 323K)

Cu^0 dose (g)	K_1 at 298K	K_2 at 323K	ΔH° (kJ/mol)
	Water		
0.035	1.75	0.146	-79.46
0.025	1.10	0.111	-73.43
0.015	0.824	0.066	-80.66
0.005	0.422	0.045	-71.60

Table 3.10: The values of ΔH^0 associated with removal of MO from the two solutions (W, W-E) at 4 Fe-Cu NPs doses at two temperatures (298 K, 323K)

Fe-Cu dose (g)	K_1 at 298 K	K_2 at 323 K	ΔH° (kJ/mol)
	Water		
0.035	0.87	2.20	29.73
0.025	0.66	1.70	30.05
0.015	0.35	0.91	30.52
0.005	0.22	0.31	10.25
	W-E		
Fe-Cudose (g)	K_1 at 298K	K_2 at 323K	ΔH° (kJ/mol)
0.035	0.090	0.33	42.22
0.025	0.074	0.23	36.65
0.015	0.070	0.14	24.21
0.005	0.030	0.055	18.28

The positive values of ΔH^o obtained for using Fe^0 and Fe-Cu in the removal of MO from water and water-ethanol solutions indicate an endothermic sorption process.[115] In the case of using Cu^0 NPs for removal of MO from water solutions, the negative values of ΔH^o are indicative of an exothermic process.

Endothermic sorption is usually associated with systems in which the energy requirement of dehydration effects of the adsorbate molecules is larger than the energy associated with the

intrinsic sorption step on the adsorbent surface. This situation is reversed if exothermic behavior is observed.

The calculated values of enthalpy change are in energy ranges which correspond mostly to physical adsorption, and in some cases, to weak chemical adsorption.[116]

It was reported in the literature, that the adsorption enthalpy, ranging from 2.1 to 20.9 kJ/mol, corresponds to a physical adsorption.[116] Thus, in case with water solutions, The values of ΔH^{o} as shown from Tables 3.8 and 3.10 are in the range of (27.4– 62.4 kJ/mol) and (10.2– 30.5 kJ/mol) for Fe^0 NPs and Fe-Cu NPs, correspondingly. This suggests that the adsorption of MO on Fe0 NPs can be classified as chemical adsorption and physical adsorption in the case of Fe-Cu NPs at lower dose (0.005g) and chemical adsorption at higher Fe-Cu doses.

3.3.4 Salinity Effect

The composition of the real dye wastewater is always complex. The dyeing wastewater includes lots of inorganic salts, and this justifies studying the effect of salinity on the removal process of MO. Four conentrations of NaCl (10, 20, 30 and 40 g/L) in 100 mg/L MO solutions (in W and W-E solvents) were used. These solutions were mixed with 35 mg samples of nanoparticle materials (Fe^0, Cu^0 and Fe-Cu), and were kept in thermostated shaking water bath at 298 K for four hours. The results of the experiments are shown in Tables 3.11& 3.12.

It can be seen that NaCl harmed decolorization of MO by Fe^0 and Cu^0 NPs. The percentage removal of MO from water by Fe^0 decreased from 94.0% to 83.6% when the concentration of NaCl was 10 g/L, and the extent of dye removal decreased further as the concentration of NaCl increased, and reached to 74.5% when the concentration of NaCl was 30 g/L. Moreover, the addition of NaCl caused a decrease in the extent of dye removal by Fe^0 in W-E mixture from 33.5% to 0%. This might be caused by the outside iron oxide layer in Fe^0 NPs which is positively charged under the isoelectric point, which is accessible to the anions that have atoms with a lone pair of electrons such as chloride ions. These ions could compete with MO in occupying the adsorptive and reactive sites of the Fe^0 NPs surfaces, thus leading to a decrease of the decolorization efficiency.[45] The same results were obtained when Cu^0 is used; the percentage removal of MO from water decreased from 63.6% to 57.1% when the concentration of NaCl was 20 g/L.

In contrast to Fe^0 and Cu^0, the percentage removal of MO from water by Fe-Cu NPs increased from 46.5% to 71.4 % when the concentration of NaCl was 30 g/L. This may be referred to the assumption that, sometimes the counter ions of the salt may reduce the surface charge, and may reduce the repulsions between the elements of same charge, and thus increase the adsorption efficiency. This behavior requires further investigation.

Table 3.11: Salinity effect when water is used as a solvent

Fe^0			
NaCl Conc.(g/L)	C (mg/L)	Q (mg/g)	% Removal
10	16.4	59.7	83.6
20	21.5	56.0	78.5
30	25.4	53.3	74.5
40	18.2	58.4	81.8
Cu^0			
10	42.5	41.0	57.5
20	42.9	40.8	57.1
30	41.4	41.8	58.6
40	41.3	41.9	58.7
Fe-Cu			
10	48.4	36.8	51.6
20	43.2	40.6	56.8
30	28.6	51.0	71.4
40	31.7	48.8	68.3

Table 3.12: Salinity effect when water and ethanol (50%:50%) mixture is used as a solvent

Fe^0			
NaCl Conc. (g/L)	C (mg/L)	Q (mg/g)	% Removal
10	96.7	2.4	3.3
20	99.7	0.2	0.3
30	100	0	0.0
40	100	0	0.0
Cu^0			
10	98.5	1.0	1.5
20	98.6	1	1.4
30	99.4	0.4	0.6
40	100	0	0.0

3.3.5 Heterogeneous Fenton Reaction

In this section, Fe^0, Cu^0 and Fe-Cu NPs were used as a Fenton-like catalyst in the removal of MO. The experiments were conducted in W and in W-E solutions at 100 mg/L MO initial concentration.

Heterogeneous Fenton reaction is an oxidation process that has been widely studied in organic wastewater treatment. This method is based on the generation of hydroxyl radicals (HO·), which have a strong oxidation capacity. In heterogeneous Fenton oxidation, solid metal-catalysts can catalyze the decomposition of H_2O_2 with the production of highly reactive OH radical. Thus, complex organic molecules can be either oxidized by HO· to smaller organics or completely mineralized to carbon dioxide (CO_2) and water (H_2O).[117,118] The production of the radicals, using Fe NPs as a catalyst, can be represented by:[80]

$$Fe^0 + O_2 \xrightarrow{H+} Fe^{2+} + H_2O_2$$

$$Fe^0 + H_2O_2 \rightarrow Fe^{2+} + 2H_2O_2$$

$$Fe^{2+} + H_2O_2 \rightarrow Fe^{3+} + OH^{\cdot} + OH^{-}$$

Metallic iron has been widely used as a heterogeneous Fenton catalyst. In addition, it was reported that Copper also exhibited high reactivity toward H_2O_2 over a wide pH range.[118]

The results of the related experiments are given in Figure 3.15. The figure shows that water forms a much better medium for the Fenton-like cycle, and that leads to more degradation of MO in comparison with water-ethanol mixture. This can be attributed to that, in addition to oxidizing the dye, the hydroxyl radicals produced by the Fenton cycle in acidic media can also oxidize ethanol to acetaldehyde.[119] Also the results show that Fe^0 NPs are much more effective for dye removal than Cu^0 or Fe-Cu NPs from both types of solvents. At the same time this oxidative process seems to offer no advantages over the direct use of Fe^0 NPs in the removal of MO under the studied conditions, also a higher NPs quantity (50 mg) does not give better results.

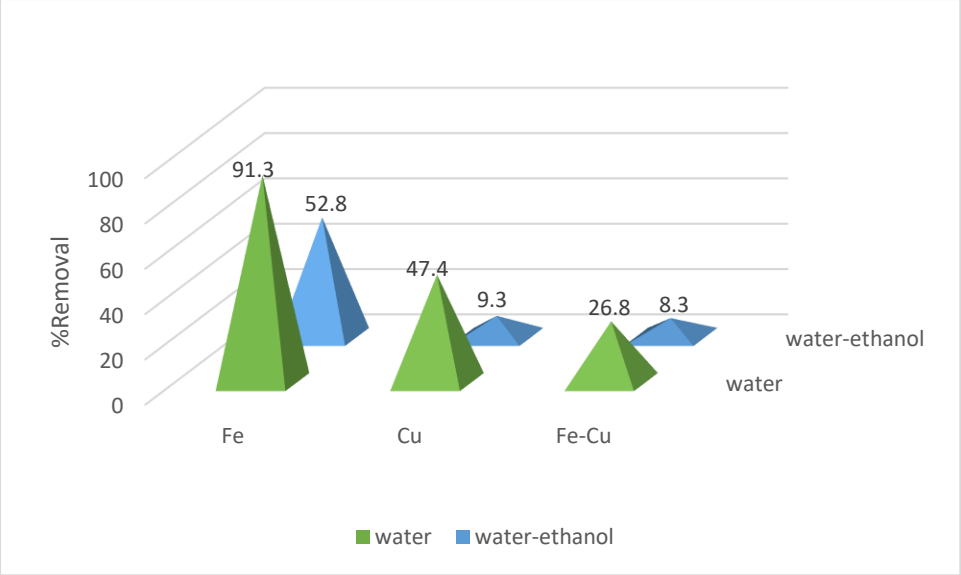

Figure 3.15: % removal of MO with Fe^0, Cu^0 and Fe-Cu NPs as a Fenton-like catalysts.

3.3.6. Effect of Time

The kinetic studies were carried out in two solvents; W and W-E, for Fe NPs and Cu NPs. The experiments were conducted at MO initial concentration of 100 mg/L for different periods of time starting from 1 min. up to 4 hours.

Based on the results presented in Figures 3.16 and 3.17, the following two conclusions can be drawn:

(i) The removal of MO is faster and more efficient in water medium compared with water-ethanol medium.

(ii) Fe NPs material is much more efficient in MO removal than Cu NPs, in both solvent systems.

Both observations are inline with the earlier conclusions reported in the previous sections regarding the extent of MO sorption.

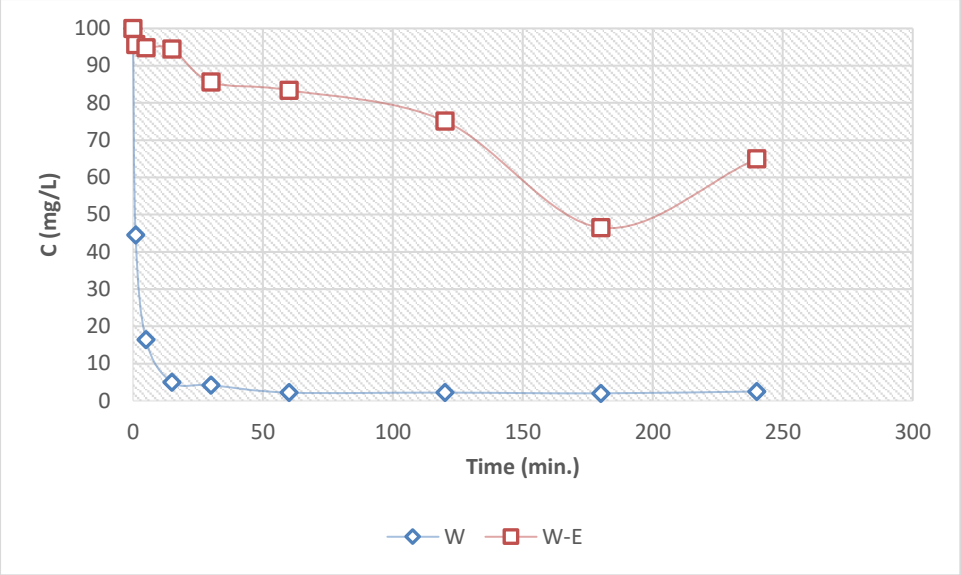

Figure 3.16: The variation of MO concentration with time at 323 K when Fe NPs are used in the MO removal in both solvents; W and W-E.

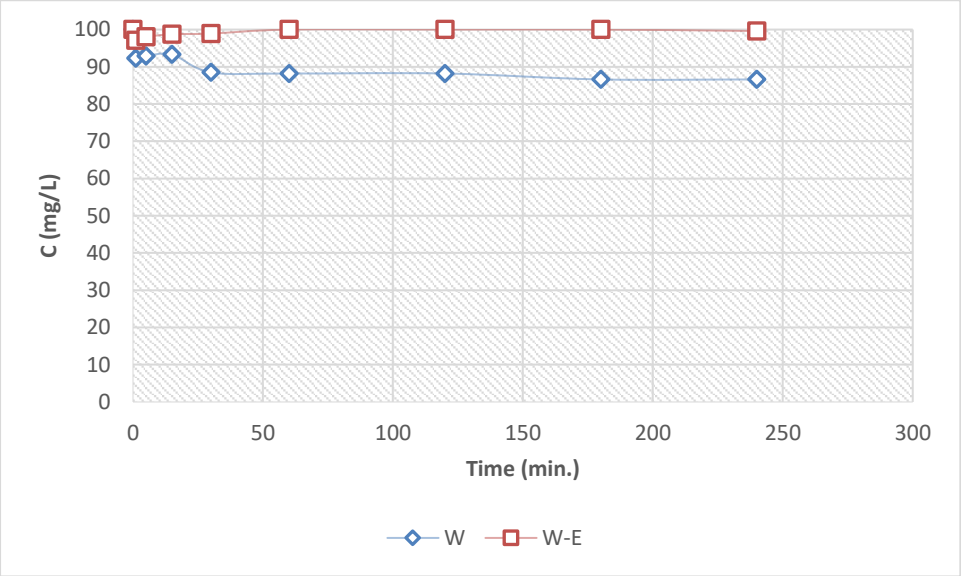

Figure 3.17: The variation of MO concentration with time at 323 K when Cu NPs are used in the MO removal in both solvents; W and W-E.

Due to the poor kinetic performance of Cu NPs, and the poor kinetic performance in W-E medium, the kinetic analysis was performed for MO removal by Fe NPs in water medium, at two operating temperatures of 298 K and 323 K. The corresponding kinetic data are shown in Table 3.13.

The expermental amount of MO removed from solution (and presumably attached to solid materials) can be calculated using the mass balance equation:

$$Q = (C_0 - C)V/m$$

Where;

Q is the removed concentration of MO (mgMO/gNPs)

C_0 is the initial concentration of MO (100 mg/L)

C is the liquid concentration of MO (mg/L) at a certain time

V is the total volume of the solution.

M is the mass of the nanoparticle material used in the removal process.

Table 3.13: Effect of time on MO removal using Fe^0 in Water at 298 K and 323K.

T = 298 K			
Time(min)	C (mg/L)	Q (mg/g)	% Removal
0	100	0	0
1	71.3	28.64	28.64
5	64.15	35.85	35.85
15	44.35	55.65	55.65
30	34.77	65.23	65.23
60	24.19	75.81	75.81
120	25.8	74.19	74.19
180	11.83	88.17	88.17
240	14.06	85.94	85.94
T = 323 K			
0	100	0	0
1	44.5	55.5	55.5
5	16.4	83.6	83.6
15	5	95	95
30	4.2	95.8	95.8
60	2.2	97.8	97.8
120	2.2	97.8	97.8
180	2	98	98
240	2.5	97.5	97.5

The data were fitted to pseudo-first and second-order kinetics. Pseudo-first-order rate equation represented by lagergren was used. The nonlinear form of lagergren equation is given as:[120]

$$Q = Q_e\ (1 - e^{-k_1 t}) \ldots\ldots\ldots\ldots (20)$$

It can be linearized to;

$$\ln(Q_e - Q\ ) = lnQ_e - k_1 \mathrm{t} \ldots\ldots\ldots\ldots (21)$$

The coefficient of determination (R^2) of the linear fits of the pseudo-first-order kinetics was very low (0.8920 at 298 K and 0.4429 at 323 K). So, it is clear that the first order kinetics is not applicable.

Next, pseudo-second-order rate equations represented by Ho Equation[121] and Shahwan Equation[122] were used. As reported by their authors, these two equations were derived using two different approaches, and although the two equations look similar to each other, they differ in the interpretation of Q_e (or Q_m) and the method of determination of the rate constant, k, and its unit. Since Q_m is used instead of Q_e, Shahwan equation was reported to provide better applicability when the removal is almost complete.

The nonlinear form of Ho equation is given as:[121]

$$Q = \frac{k_2 . t . Qe^2}{1 + k_2 . Qe . t} \ldots\ldots\ldots\ldots\ldots (22)$$

It can be linearized to;

$$\frac{t}{Q} = \frac{1}{k_2 Qe^2} + \frac{1}{Qe} t \ldots\ldots\ldots\ldots\ldots (23)$$

Where Q_e is the experimental value of Q at the equilibrium, and k is the rate constant.

On the other hand, the nonlinear and linearized forms of Shahwan's equation are given as:[122]

$$Q = \frac{Q_m C_0\, k_2 t}{C_0\, k_2 t + 1} \ldots\ldots\ldots\ldots\ldots (24)$$

$$\frac{t}{Q} = \frac{1}{Q_m C_0 K_2} + \frac{1}{Q_m} t \ldots\ldots\ldots\ldots (25)$$

Where;

C_0 is the initial concentration of the MO

k_2 is the second-order rate constant

Q is the amount of MO sorbed on NPs.

Q_m is the maximum amount of solute that would be sorbed if the sorption reaction goes to completion.

The linear fits of the kinetic data can be obtained by plotting t/Q vs t for both of Ho and Shahwan models, as shown in Figure 3.18. The high value of coefficient of determination indicates the applicability of the second-order kinetics for MO removal by Fe NPs.

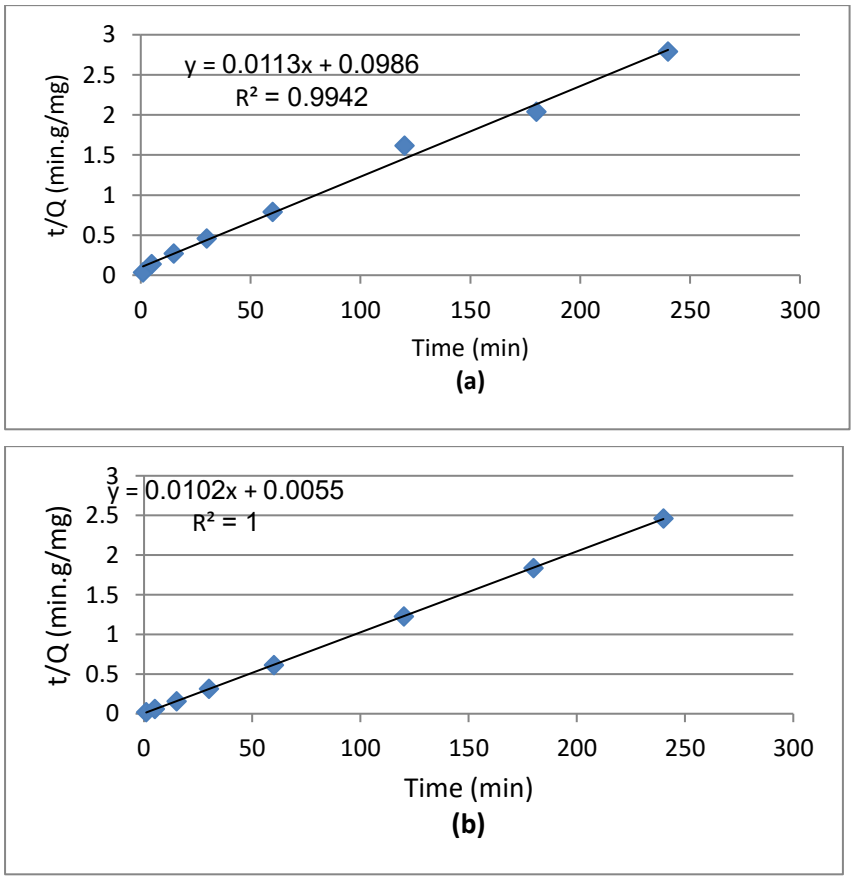

Figure 3.18: Pseudo-second-order linear fit for the removal process of MO (100 mg/L MO and 0.025g Fe^0) from water solutions using Fe NPs at: (a) 298K, (b) 323K.

The obtained kinetic prameters are given in Tables 3.14 and 3.15. The activation energy was calculated using the equation:

$$ln\frac{k_2}{k_1} = \frac{E_a}{R}\left(\frac{1}{T_1} - \frac{1}{T_2}\right) \ldots\ldots\ldots\ldots (26)$$

Table 3.14: The obtained results for the pseudo-second-order linear fit using Ho's equation.

	W at 298K	W at 323K
Slope	0.0113	0.0102
R^2	0.9942	1
Intercept	0.0986	0.0055
k_2 (g $mg^{-1}min^{-1}$.)	$1.295x10^{-3}$	0.0189
Q_e (theo) (mg/g)	88.50	98.04
Q_e (exp) (mg/g)	88.17	98
$\lvert E_a \rvert$(kJ/mol)	85.81	

Table 3.15: The obtained results for the pseudo-second-order linear fits using Shahwan's equation.

	W at 298K	W at 323K
Slope	0.0113	0.0102
R^2	0.9942	1
Intercept	0.0986	0.0055
k_2 (L$mg^{-1}min^{-1}$)	$1.146x10^{-3}$	0.0185
Q_m (theo) (mg/g) (=C_0V/M)	100	100
Q_m (exp) (mg/g)	88.17	98
$\lvert E_a \rvert$(kJ/mol)	89.40	

Alternatively, the experimental data were also fitted by nonlinear fitting using the two equations, and the results are shown in Figures 3.19 and 3.20. The obtained rate constants and the calculated activation energy values are given in Table 3.16.

Table 3.16: Rate constants and the calculated activation energy values obtained from nonlinear fit.

At 298 K	k2	$\lvert E_a \rvert$(kJ/mol)
Ho	0.0013 (g $mg^{-1}min^{-1}$.)	73.70
Shahwan	0.0011 ($Lmg^{-1}min^{-1}$)	76.50
At 323 K		
Ho	0.013 (g $mg^{-1}min^{-1}$.)	
Shahwan	0.012 ($Lmg^{-1}min^{-1}$)	

In order to compare the results of the linear fits to the results of the nonlinear fits, nonlinear plots were constructed using the data obtained from the linear fits and added into the above-mentioned figures. The results show that, when Ho equation is used, there are little difference between linear and nonlinear fits, as both of them yield values close to similar extent to the experimental values. On the other hand, when Shahwan equation is used, nonlinear fitting yields results closer to the experimental data than linear fitting, especially for the data at 298 K. Hence, nonlinear fitting would be recommended for such cases.

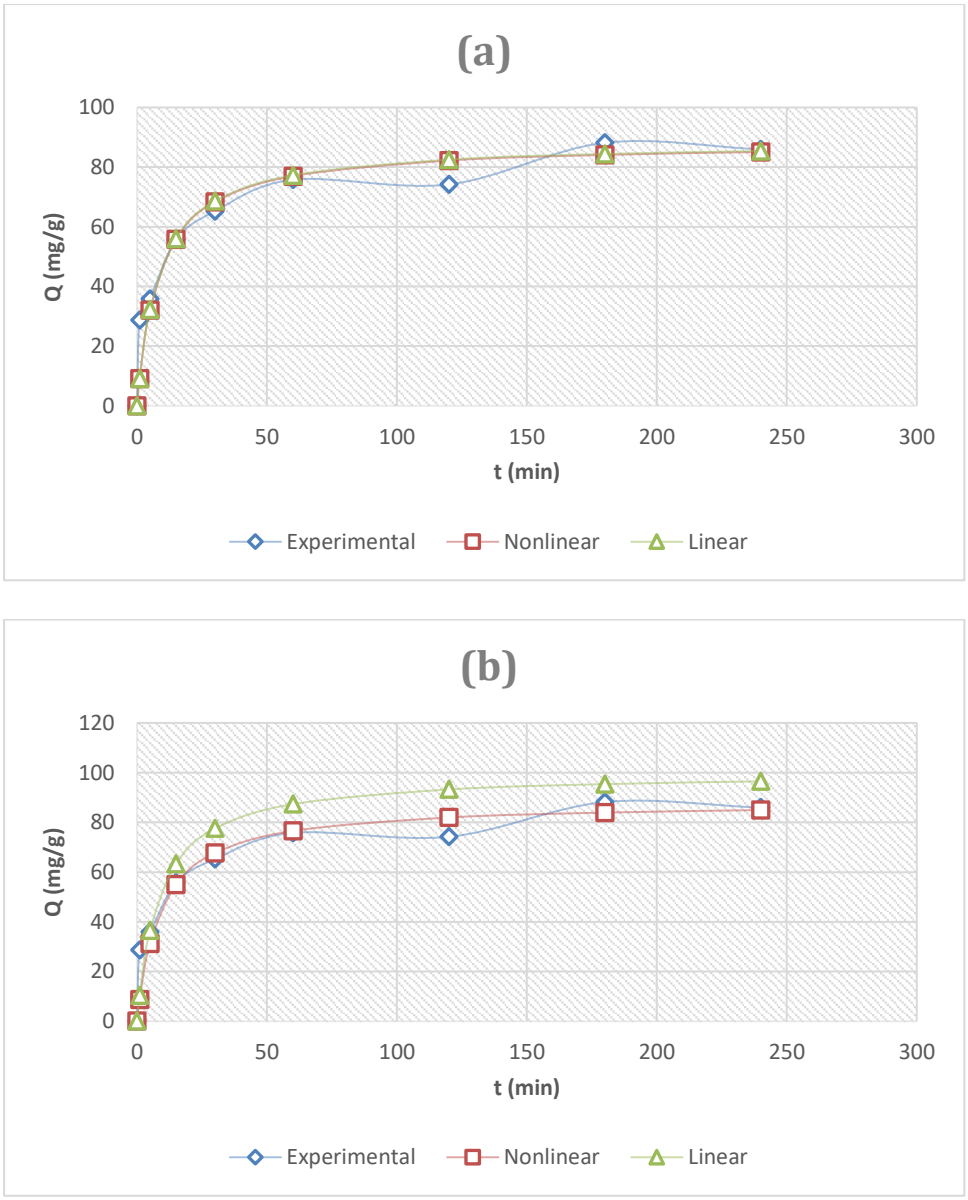

Figure 3.19: nonlinear and linear fit of the kinetic data of MO removal by Fe NPs at 298 K; (a) using Ho equation (b) using Shahwan equation.

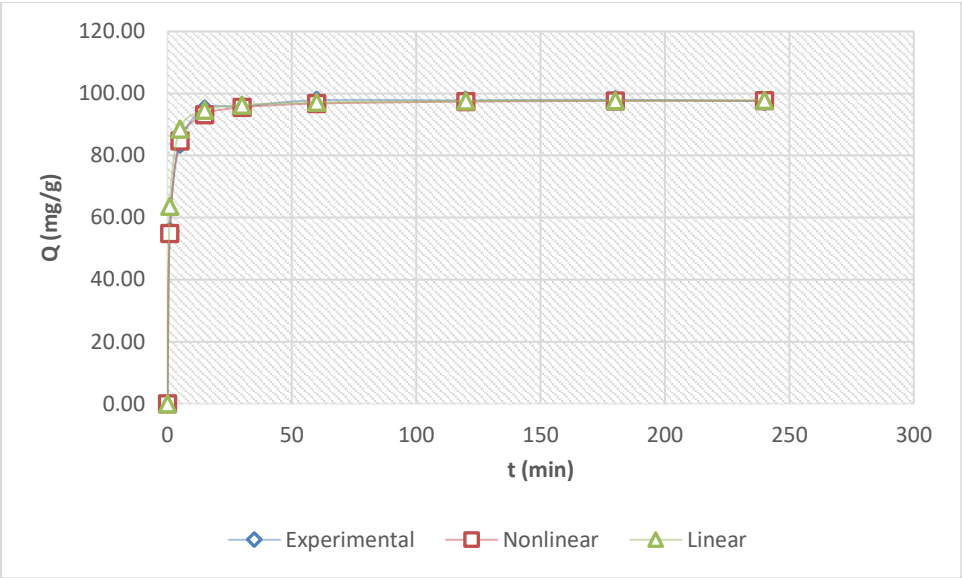

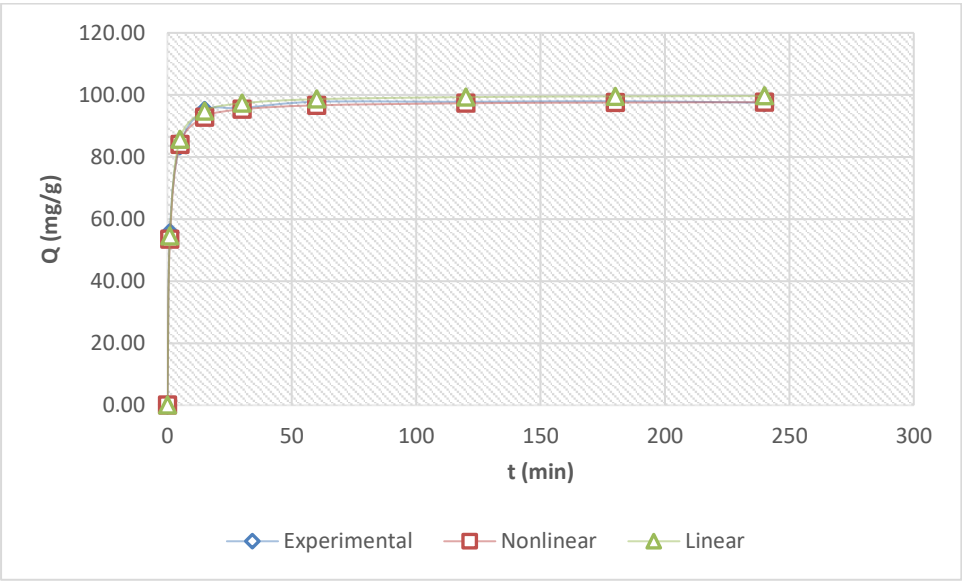

Figure 3.20: nonlinear and linear fit of the kinetic data of MO removal by Fe NPs at 323 K; (a) using Ho equation (b) using Shahwan equation.

Based on the kinetic analysis, the following conclusions can be obtained:

- Equilibrium of MO removal is achieved fast, within about an hour of contact at 298 K, and considerably less than that at 323 K.
- As can be seen from the rate constants, the rate of MO removal in the water medium is higher at higher temperature.

- The increase in rate constants with increasing temperature leads to positive activation energies. This signifies a process in which the increase in temperature leads to more activated molecules which are capable of crossing the activation energy barrier, and as such, leads eventually to accelerating the MO removal at higher temperatures.
- In all cases, the obtained Q_e values from the mathematical fitting are considerably close to experimental Q_e values, suggesting the adequacy of this model for describing the sorption system.
- The nonlinear fitting can be recommended over linear fitting.

4. Conclusion

This study has found that the transition energy of MO in the three studied solvents may be correlated with the values of dielectric constant and surface tension of these solvents. Under the studied experimental conditions, the results showed that no distinctive signs for dimers or higher order aggregates of MO are seen in the UV-Vis spectra. However, a blue shift was observed in the solutions of MO in water-ethanol and in water-DMSO relative to the MO in water. No obvious intensity changes were observed in all cases, this shows that the solute-solute interactions are less effective than the solute-solvent interactions in determining the behavior of MO molecules in solution.

By comparing the three synthesized nanoparticles, it was found that Fe NPs are more effective in dye removal than both of Cu NPs and Fe-Cu NPs under all conditions, and with a proper dose of Fe NPs, it is possible to attain almost a complete removal of MO from water. In addition, it was found generally that water solutions are distinctly more suitable than the other used solvents in this study for the removal of MO. When Fe NPs are used in MO removal, the trend of dye removal in different solvents is: water > water-ethanol > water-DMSO. This trend is proportional with the trend of polarity of the solvents. In the cases of Cu NPs and Fe-Cu NPs, almost no dye removal is observed in water-ethanol and water-DMSO solvents at 298K.

Increasing the NPs dose results in increasing the extent of removal of MO from water solutions for the three types of nanoparticles. At the same time, in water-ethanol solution increasing the dose of Cu and Fe-Cu NPs made no significant difference to the extent of MO removal. But this increase in dose reflects positively on MO removal from water-ethanol solutions when Fe NPs were used. In water solutions at 298 K, the removal of MO can be best described with Harkins-Jura isotherm and to a lesser extent by Freundlich isotherm. The same is not true when temperature is increased to 323 K.

The removal of MO from water and water-ethanol solutions using Fe NPs and Fe-Cu NPs was observed to be endothermic, but it was observed to be exothermic in the case of Cu NPs. Endothermic sorption is usually associated with systems in which the energy requirement of dehydration effects of the adsorbate molecules is larger than the energy associated with the intrinsic sorption step on the adsorbent surface. This situation is reversed if exothermic behavior is observed. The calculated values of enthalpy change are in energy ranges which correspond mostly to physical adsorption, and in some cases, to weak chemical adsorption.

The research has also shown that the addition of NaCl salt reduced the extent of MO removal, under the studied experimental conditions. The salt concentration in the solution

affects the ionic strength of the medium, and can alter its polarity and thus the interaction between dye molecules and solvent molecules.

Water forms a much better medium for the Fenton-like cycle, and that leads to more degradation of MO in comparison with water-ethanol mixture. In addition, Fe NPs are much more effective for dye removal than Cu NPs or Fe-Cu NPs from both types of solvents. However, this oxidative process seems to offer no advantages over the direct use of Fe NPs in the removal of MO under the studied conditions.

The kinetic analysis of MO removal from water using Fe NPs showed that equilibrium of dye removal is achieved fast, and that the rate constants increase with temperature, thus MO removal is accelerated at higher temperatures. The kinetic data can be described with second-order kinetics, and nonlinear fitting of the data can be recommended over linear regression.

5. References

1. Fan, Li.; Tao. Zh., Effects of objective and subjective environmental pollution on well-being in urban China: A structural equation model approach. *Social Science & Medicine.* **2020***, 249,* 112859-112867.
2. Iyyanki, V.; Muralikrishna; Valli, M., *Environmental Management Science and Engineering for Industry*, Published by Elsevier Inc. India, **2017**.
3. Prince, O.; Ukaogo; Chibuzo,V.; Onwuka, Environmental pollution: causes, effects, and the remedies. *Microorganisms for Sustainable Environment and Health,* **2020,** *21***,** 419-129.
4. Safoura, S.; Jamil, A., Environmental pollution and geo-ecological risk assessment of theQhorveh mining area in western Iran. *Environ. Pollut.* **2019**, *253*,811-820.
5. Lygia, Th.; Budnik; Ludwine, C.; Anastasia, K.; Paschalidou; Pavlos, K., Pollution in living and working environments, climate variability, and their impact on non-communicable disease burden. *Sci. Total Environ.* **2019**, *660*, 593-594.
6. Rene, P.; Schwarzenbach; Thomas, E.; Thomas, B.; Hofstetter; Urs, G. and Bernhard, W., Global Water Pollution and Human Health. *Annu. Rev. Environ. Resour.* **2010**, *35*, 109-136.
7. Sheenam, Th.; Rohit,V.; Parul, Kh., Water Quality Standards, Its Pollution and Treatment Methods. *A New Generation Material Graphene: Applications in Water Technology.* Springer, Cham., India, **2019.**
8. Partha, S.; Aamod,V.; Desai; Sumanta, L.; Sujit, K.; Ghosh, Advanced Porous Materials for Sensing, Capture and Detoxification of Organic Pollutants toward Water Remediation. *ACS Sustainable Chem. Eng.* **2019**, *7*, 7456−7478.
9. Yong, Z.; Lei, Z.; Zhengjun, Ch., Removal of organic pollutants from aqueous solution using agricultural wastes: A review. *J. Mol. Liq.*, **2015**, *212*, 739–762.
10. Yanbo, Z.; Jian, Lu.; Zhou, Y.; Yongdi, L., Recent advances for dyes removal using novel adsorbents: A review. *Environ. Pollut.* **2019**, *252*, 352-365.
11. Chequer, D.; Maria, F.; Oliveira, G. A. R.; Ferraz, E. R. A.; Carvalho, J.; Zanoni, M. V.B.; Oliveir, D. P., "Textile Dyes: Dyeing Process and Environmental Impact." in *Eco-Friendly Textile Dyeing and Finishing*. InTech. **2013**.
12. Gürses; Ahmet; Açıkyıldız, M.; Güneş, K.; Gürses, S., Dyes and Pigments: Their Structure and Properties. Springer, **2016**.

13. Asiri, Abdullah, M., Organometallic Dyes: Part 1. Synthesis of Orange to Cyan Dyes Based on Donor-Conjugated-Acceptor Chromogenes Using Ferrocene as the Donor Group. *Appl. Organomet. Chem.* **2001**,*15*, 907–915.
14. Rane, A.; Joshi, S. J., Biodecolorization and Biodegradation of Dyes: A Review. *Open Biotechnol. J.* **2021**,*15*, 97–108.
15. Carmen, Z.; Daniel, S., Textile Organic Dyes – Characteristics, Polluting Effects and Separation/Elimination Procedures from Industrial Effluents – A Critical Overview. *Org. Pollut. Ten Years After Stock. Conv. - Environ. Anal. Updat.* **(2012)** doi:10.5772/32373.
16. Bafana, A.; Devi, S. S.; Chakrabarti, T., Azo dyes: Past, present and the future. *Environ. Rev*. **2011**, *19*, 350–370.
17. Natarajan, S.; Bajaj, H. C. & Tayade, R. J., Recent advances based on the synergetic effect of adsorption for removal of dyes from waste water using photocatalytic process. *J. Environ. Sci. (China)*, **2018**,*65*, 201–222.
18. Wu, L.; Liu, X.; Lv, G.; Zhu, R.; Tian, L.; Liu, M.; Li, Y.; Rao, W.; Liu, T.; Liao, L., Study on the adsorption properties of methyl orange by natural one-dimensional nano-mineral materials with different structures. *Sci. Rep.* **2021**, *11*, 1–11.
19. Kant, R., Textile dyeing industry an environmental hazard. *Nat. Sci.*, **2012**, *04*, 22–26.
20. Rashid, T. U.; Kabir, S. M. F.; Biswas, M. C.; Bhuiyan, M. A. R., Sustainable Wastewater Treatment via Dye-Surfactant Interaction: A Critical Review. *Ind. Eng. Chem. Res.* **2020** ,*59*, 9719–9745.
21. Osagie, C.; Othmani, A.; Ghosh, S.; Malloum, A.; Esfahani, Z. K.; Ahmadi, Ah., Dyes adsorption from aqueous media through the nanotechnology: A review. *J. Mater. Res. Technol.* **2021**, *14*, 2195–2218.
22. Azami, M.; Bahram, M.; Nouri, S.; Naseri, A.; A central composite design for the optimization of the removal of the azo dye, Methyl Orange, from waste water using the Fenton reaction. *J. Serbian Chem. Soc.* **2012**, *77*, 235–246.
23. Hao, O. J.; Kim, H.; Chiang, P. C., Decolorization of wastewater. *Crit. Rev. Environ. Sci. Technol.* **2000,** *30*, 449–505.
24. Sonune, A.; Ghate, R., Developments in wastewater treatment methods. *Desalin. A. Sonune, R. Ghate / Desalin.* **2004**, ***167***, 55–63.

25. Kasperchik, V. P.; Yaskevich, A. L.; Bil'Dyukevich, A. V., Wastewater treatment for removal of dyes by coagulation and membrane processes. *Pet. Chem.* **2012**,*52*, 545–556.
26. Luo, X.; Liang, C.; Hu, Y., Comparison of different enhanced coagulation methods for azo dye removal from wastewater. *Sustain.* **2019**, *11*, 1–14.
27. Hassan, M. M.; Carr, C. M., A critical review on recent advancements of the removal of reactive dyes from dyehouse effluent by ion-exchange adsorbents. *Chemosphere*. **2018,** *209*, 201–219.
28. Wang, S.; Zhu, Z. H., Characterisation and environmental application of an Australian natural zeolite for basic dye removal from aqueous solution. *J. Hazard. Mater*. **2006**, *136*, 946–952.
29. **Petriciolet**, A. B.; Castillo; Didilia, I. M.; Dotto, G. L.; Duran-Valle, C. J.,"ADSORPTION IN WATER TREATMENT". Reference Module in Chemistry, Molecular Sciences and Chemical Engineering. Elsevier, **2019**.
30. Awad, A. M.; Jalab ,R.; Benamor.A.; Nasser, M.S.; Ba-Abbad, M. M.; El-Naas, M.; Mohammad, A.W., Adsorption of organic pollutants by nanomaterial-based adsorbents: An overview. *J. Mol. Liq.* **2020**,*301*, 112335, 1-31.
31. Xiao, W.; Jiang, X.; Liu, X.; Zhou, W.; Garba, Z.N.; Lawan, I.; Wang, L.; Yuan, Z., Adsorption of organic dyes from wastewater by metal-doped porous carbon materials. *J. Clean. Prod.* **2021**, *284*, 124773,1-20.
32. Zainal Abidin, A.; Abu Bakar, N. H. H.; Ng, E. P.; Tan, W. L., Rapid Degradation of Methyl Orange by Ag Doped Zeolite X in the Presence of Borohydride. *J. Taibah Univ. Sci.* **2017**, *11*, 1070–1079.
33. Corda, N. C.; Kini, M. S., A Review on Adsorption of Cationic Dyes using Activated Carbon. *MATEC Web Conf.* **2018,** *144* (02022)1-16.
34. Djilani, Ch.; Zaghdoudi, R.; Djazi, F.; Bouchekima, B.; Lallam, A.; Modarressi, A.; Rogalski, M., Adsorption of Dyes on Activated Carbon Prepared from Apricot Stones and Commercial Activated Carbon. *J. Taiwan Inst. Chem. Eng.* **2015**, *53*, 112–121.
35. Batool, S.; Akib, S.; Ahmad, M.; Balkhair, K. S.; Ashraf, M. A., Study of modern nano enhanced techniques for removal of dyes and metals. *J. Nanomater.* **2014**, *2014*,1-21.

36. Cai, Z.; Sun, Y.; Liu, W.; Pan, F.; Sun, P.; Fu, J., An Overview of Nanomaterials Applied for Removing Dyes from Wastewater. *Environ. Sci. Pollut. Res.* **2017**, *24*, 15882–15904.
37. Homaeigohar, S., The nanosized dye adsorbents for water treatment. *J. Nanomater*. **2020**, *10*, 1-43.
38. Tara, N.; Siddiqui, S. I.; Rathi, G.; Chaudhry, S.A.; Inamuddin; Asiri, A. M., Nano-Engineered Adsorbent for the Removal of Dyes from Water: A Review. *Curr. Anal. Chem.* **2019**, *16*, 14–40.
39. Kale, R. D.; Kane, P. B., Colour removal using nanoparticles. *Text. Cloth. Sustain.* **2017**, *2*,1-7.
40. Sadegh, H.; Ali, G.A. M.; Gupta, V. K.; Makhlouf, A. S.H.; ghoshekandi, R.S.; Nadagouda, M. N.; Sillanpa, M.; Megiel, E., The role of nanomaterials as effective adsorbents and their applications in wastewater treatment. *J. Nanostructure Chem.* **2017**,*7*, 1–14.
41. Lefevre, E.; Bossa, N.; Wiesner, M. R.; Gunsch, C. K., A review of the environmental implications of in situ remediation by nanoscale zero valent iron (nZVI): Behavior, transport and impacts on microbial communities. *Sci. Total Environ*. **2016**, *565*, 889-901.
42. Nairat, M.; Shahwan, T.; Eroglu, A.E.; Fuchs, H., Incorporation of iron nanoparticles into clinoptilolite and its application for the removal of cationic and anionic dyes. *J. Ind. Eng. Chem.* **2015**,*21*, 1143–1151.
43. Shahwan, T.; Abu Sirriah, S.; Nairat, M.; Boyacı, E.; Eroğlu, A.E.; Scott, T.B.; Hallam, K.R., Green synthesis of iron nanoparticles and their application as a Fenton-like catalyst for the degradation of aqueous cationic and anionic dyes. *Chem. Eng. J.* **2011**, *172*, 258-266.
44. Cristiana, R.; Gustavo, A.; Mayra, A.; André, F., Degradation of the Reactive Blue 4 Dye in Aqueous Solution Using Zero-Valent Copper Nanoparticles. *J. Nanomater.* **2018**, *2018*,1-9.
45. Jing, F.; Yanhui, G.; Jianji, W.; Maohong, F., Rapid decolorization of azo dye methyl orange in aqueous solution by nanoscale zerovalent iron particles. *J.Hazard.Mater*. **2009**, *166*, 904–910.
46. Al-Bastaki, N., Removal of methyl orange dye and Na2so4 salt from synthetic waste water using reverse osmosis. *Chem. Eng. Process. Process Intensif.* **2004**,*43*, 1561–1567.

47. de Oliveira, H. P.; Oliveira, E. G. L.; de Melo, C. P., Aggregation of methyl orange probed by electrical impedance spectroscopy. *J. Colloid Interface Sci.* **2006**, *303*, 444–449.
48. Bazrafshan, E.; Zarei, A. A.; Nadi, H.; Zazouli, M. A., Adsorptive removal of Methyl Orange and Reactive Red 198 dyes by Moringa peregrina ash. *Indian J. Chem. Technol.* **2014**, *21*, 105-113.
49. Agarwal; Anuja; Vaishali., Removal of methyl orange dye from textile effluent using adsorption on chitosan hydrogel beads. *ESSENCE - International Journal for Environmental Rehabilitation and Conservation*. **2016**, *2*, 73 – 80.
50. https://www.chemguide.co.uk/physical/acidbaseeqia/indicators.html (accessed Oct, 18th 2021)
51. https://en.wikipedia.org/wiki/Methyl_orange (accessed Oct, 18th 2021)
52. Del Nero, J.; De Araujo, R. E.; Gomes, A. S. L.; De Melo, C. P., Theoretical and experimental investigation of the second hyperpolarizabilities of methyl orange. *J. Chem. Phys.* **2005** ,*122(*104506*)*, 1-7.
53. Giri, M. K.; Jaggi, N., Absorption and Fluorescence Spectra of Methyl Orange in Aqueous Solutions View project. *ANNO LXVII*. **2012**, *2*, 256-261.
54. https://www.britannica.com/science/iron-chemical-element **(**accessed Oct, 19th 2021)
55. https://web.archive.org/web/20060417160321/http://www.mii.org/Minerals/photoiron.html (accessed Oct, 19th 2021)
56. https://en.wikipedia.org/wiki/Iron_ore#cite_ref-1 (accessed Oct, 19th 2021)
57. Guan, X.; Sun, Y.; Qin, H.; Li, J.; Di He, M.C.; Dong, H., The limitations of applying zero-valent iron technology in contaminants sequestration and the corresponding countermeasures: The development in zero-valent iron technology in the last two decades (1994-2014). *Water Res*. **2015**,*75*, 224-248.
58. Mukherjee, R.; Kumar, R.; Sinha, A.; Lama, Y.; Saha, A. K., A review on synthesis, characterization, and applications of nano zero valent iron (nZVI) for environmental remediation. *Crit. Rev. Environ. Sci. Technol.* **2016**, *46*, 443–466.
59. Hu, R.; Yang, H.; Tao, R.; Cui, X.; Xia, M.; Amoah, B. K.; Cao, V.; Lufingo, M.; Paloma, N.; Ndé-Tchoupé, A. I.; Gatcha-Bandjun, N.; Tala, V. R. S.; Gwenzi, W.; Noubactep, C., Metallic iron for environmental remediation: Starting an overdue progress in knowledge(review). *Water (Switzerland)*. **2020**, *12(3)*,1-26.

60. Galdames, A.; Ruiz-Rubio, L.; Orueta, M.; Sánchez-Arzalluz, M.; Vilas-Vilela, J. L., Zero-valent iron nanoparticles for soil and groundwater remediation. *Int. J. Environ. Res. Public Health*. **2020**, ***17***, 1–23.
61. Crane, R. A.; Scott, T. B., Nanoscale zero-valent iron: Future prospects for an emerging water treatment technology. *J. Hazard. Mater.* **2012**,*211–212*, 112–125.
62. Machado, S.; Pacheco, J. G.; Nouws, H. P. A.; Albergaria, J. T.; Delerue-Matos, C., Characterization of green zero-valent iron nanoparticles produced with tree leaf extracts. *Sci. Total Environ.* **2015**, *533*, 76–81.
63. Sun, Y. P.; Li, X. Q.; Cao, J.; Zhang, W. X.; Wang, H. P., Characterization of zero-valent iron nanoparticles. *Adv. Colloid Interface Sci*. **2006**, *120*,47–56.
64. https://www.britannica.com/science/copper (accessed Oct, 20th 2021)
65. https://en.wikipedia.org/wiki/Copper (accessed Oct, 20th 2021)
66. Gawande, M. B.; Goswami, A.; Felpin, F. X.; Asefa, T.; Xiaoxi, H.; Silva, R.; Zou, X.; Zboril, R.; Varma, R.S., Cu and Cu-Based Nanoparticles: Synthesis and Applications in Catalysis. *Chem. Rev.* **2016**,*116*, 3722–3811.
67. Din, M. I.; Rehan, R., Synthesis, Characterization, and Applications of Copper Nanoparticles. *Anal. Lett.* **2017**, *50* ,50–62.
68. Sinha, T.; Ahmaruzzaman, M., Green synthesis of copper nanoparticles for the efficient removal (degradation) of dye from aqueous phase. *Environ. Sci. Pollut. Res.* **2015**,*22*, 20092–20100.
69. Usman, M. S.; ElZowalaty, M. E.; Shameli, k.; Zainuddin, N.; salama, M.; Ibrahim, N. A., Synthesis, characterization, and antimicrobial properties of copper nanoparticles. *Int. J. Nanomedicine*. **2013**,*8*, 4467–4479.
70. Ali, N.; Awais, Kamal, T.; Islam, M.; Khan, A.; Shah, S. J.; Zada, A., Chitosan-coated cotton cloth supported copper nanoparticles for toxic dye reduction. *Int. J. Biol. Macromol.* **2018**, *111*, 832–838.
71. Tamilvanan, A.; Balamurugan, K.; Ponappa, K.; Kumar, B. M., Copper nanoparticles: Synthetic strategies, properties and multifunctional application. *Int. J. Nanosci.* **2014**,*13*,1-22.
72. Sharma, G.; Kumar, A.; Sharma, S.; Naushad, M.; Dwivedi, R. P.; ALOthman, Z. A.; Mola, G. T.; Novel development of nanoparticles to bimetallic nanoparticles and their composites: A review. *J. King Saud Univ. - Sci.* **2019**, ***31***, 257–269.
73. Swiatkowska, W. Z., Bimetal CuFe Nanoparticles—Synthesis, Properties, and Applications. *Appl. Sci.* **2021**, *11*, 1-15.

74. Nasrabadi, H. T.; Abbasi, E.; Davaran, S.; Kouhi, M.; Akbarzadeh, A., Bimetallic nanoparticles: Preparation, properties, and biomedical applications. *Artif. Cells, Nanomedicine Biotechnol.* **2016**, *44*, 376–380.
75. Blosi, M.; Ortelli, S.; Costa, A.L.; Dondi, M.; Lolli, A.; Andreoli, S.; Benito, P.; Albonetti, S., Bimetallic nanoparticles as efficient catalysts: Facile and green microwave synthesis. *Materials (Basel).* **2016** ,*9*, 1–25.
76. Gunawardana, B.; Singhal, N.; Swedlund, P., Degradation of chlorinated phenols by zero valent iron and bimetals of iron: A review. *Environ. Eng. Res.* **2011**,*16*, 187–203.
77. Mazhar, T.; Shrivastava, V.; Tomar, R. S., Green synthesis of bimetallic nanoparticles and its applications: A review. *J. Pharm. Sci. Res.* **2017**, *9*, 102–110.
78. Kumari,N.; Kour, S.; Singh, G.; Chauhan, A.; Verma, R.; Sharma, R.K., A brief review on the synthesis of bimetallic nanoparticles for biomedical and solar energy applications. *AIP Conf. Proc.* **2020**, *2220*,1-6.
79. Gautam, R. K.; Chattopadhyaya, M. C., Bimetallic Nanomaterials for Remediation of Water and Wastewater. *Nanomater. Wastewater Remediat.* **2016**, 273–295.
80. Liu, W. J.; Qian, T. T.; Jiang, H., Bimetallic Fe nanoparticles: Recent advances in synthesis and application in catalytic elimination of environmental pollutants. *Chem. Eng. J.* **2014**,*236*, 448–463.
81. Iwuozor, K. O.; Ighalo, J. O.; Emenike, E. C.; Ogunfowora, L. A.; Igwegbe, C. A., Adsorption of methyl orange: A review on adsorbent performance. *Curr. Res. Green Sustain. Chem.* **2021**, *4* (100179), 1-16.
82. Heidarinejad, Z.; Dehghani, M. H.; Heidari, M.; Javedan, G.; Ali, I.; Sillanpää, M.; Received: Methods for preparation and activation of activated carbon: *a review. Environ. Chem. Lett* .**2020**, *18*, 393–415.
83. Borsagli, F. G. L.; Ciminelli, V. S. T.; Ladeira, C. L.; Haasc, D. J.; Lagec, A. P.; Mansur, H. S., Multi-functional eco-friendly 3D scaffolds based on N-acyl thiolated chitosan for potential adsorption of methyl orange and antibacterial activity against Pseudomonas aeruginosa. *J. Environ. Chem. Eng.* **2019**,*7*, 1-13.
84. Debnath, A.; Deb, K.; Chattopadhyay, K. K.; Saha, B., Methyl orange adsorption onto simple chemical route synthesized crystalline α-Fe2O3 nanoparticles: kinetic, equilibrium isotherm, and neural network modeling. *Desalin. Water Treat.* **2016**, *57*, 13549–13560.

85. Kumar, K. Y.; Archana, S.; Raj, T. N. V.; Prasana, B. P.; Raghu, M. S.; Muralidhara, H. B., Superb adsorption capacity of hydrothermally synthesized copper oxide and nickel oxide nanoflakes towards anionic and cationic dyes. *J. Sci. Adv. Mater. Devices*. **2017**, *2*, 183–191.
86. Lin, D.; Zhang, Z.; Hu, L., Adsorption Models of Groundwater Remediation by Nanoscale Zero Valent Iron Proceedings of the 8th International Congress on Environmental Geotechnics. *Environ. Sci. Eng*. **2019**,*1*,512-520.
87. Chen, Z. X.; Jin, X. Y.; Chen, Z.; Megharaj, M.; Naidu, R., Removal of methyl orange from aqueous solution using bentonite-supported nanoscale zero-valent iron. *J. Colloid Interface Sci.* **2011**,*363*, 601–607.
88. Yoon, S.; Bae, S., Novel synthesis of nanoscale zerovalent iron from coal fly ash and its application in oxidative degradation of methyl orange by Fenton reaction. *J. Hazard. Mater.* **2019**,*365*, 751–758.
89. Ismail, M.; Gul, S.; Khan, M. I.; Khan, M. A.; Asiri, A. M.; Khan, S. B., Green synthesis of zerovalent copper nanoparticles for efficient reduction of toxic azo dyes congo red and methyl orange. *Green Process. Synth.***2019**, *8*, 135–143.
90. Alani, O. A.; Ari, H. A.; Offiong, N. A. O.; Alani, S. O.; Li, B.; Zeng, Q. R.; Feng, W., Catalytic Removal of Selected Textile Dyes Using Zero-Valent Copper Nanoparticles Loaded on Filter Paper-Chitosan-Titanium Oxide Heterogeneous Support. *J Polym Environ*. **2021**,*29***,** 2825–2839.
91. Lu, F.; Astruc, D., Nanocatalysts and other nanomaterials for water remediation from organic pollutants. *Coord. Chem. Rev.* **2020**,*408*, 1-31.
92. Kgatle, M.; Sikhwivhilu, K.; Ndlovu, G.; Moloto, N., Degradation Kinetics of Methyl Orange Dye in Water Using. *Catalysts*. **2021**,*11*,1-23.
93. S. Basu, S. K.; Ghosh, S.; Kundu, S.; Nath, S.; Panigrahi, S.; Praharaj, T. Pal., Studies on the ion-association of methylene blue and salicylic acid in neat and mixed binary solvents. *Chem. Phys. Lett.* **2005**,*407*, 493–497.
94. Glavee, G. N.; Klabunde, K. J.; Sorensen, C. M.; Hadjipanayis, G. C., Chemistry of Borohydride Reduction of Iron(II) and Iron(III) Ions in Aqueous and Nonaqueous Media: Formation of Nanoscale Fe, FeB, and Fe2B Powders. *Inorganic Chemistry*. **1995** ,*34* (1), 28-35.
95. Wang, H.; Kong, H.; Zheng, J.; Peng, H.; Cao, C.; Qi, Y.; Fang, K.; Chen, W**.;** Wang, Systematically Exploring Molecular Aggregation and Its Impact on Surface Tension and Viscosity in High Concentration Solutions. *Molecules*. **2020**, *25*, 1588.

96. Park, J. Y.; Hirata, Y.; Hamada, K., Dye aggregation and interaction of dyes with a water-soluble polymer in ink-jet ink for textiles. *Color. Technol.* **2012**, *128*, 184–191.
97. Eltaboni, F.; Hemdan, S.; Ali, F. K., Spectral Parameters of Methyl Orange Interacted with Ethanol-Water Mixtures. *Global Libyan journal*. **2017,** *27*,1-8.
98. Mahmood, T. A.; Mahmood, I.; Kishwar, F.; Wahab, A., Solvatochromic effect of Methylene Blue in different solvents with different polarity. *European Academic Research*. **2013**, *1 (6)*, 1100–1109
99. Reeves, R. L.; Kaiser, R. S.; Maggio, M. S.; Sylvestre, E. A.; Lawton, W. H., Analysis of the Visual Spectrum of Methyl Orange in Solvents and in Hydrophobic Binding Sites. *Can. J. Chem.* **1973**,*51*, 628-635.
100. Shahwan, T.; Anjass, M.; Naser, R., Discoloration of Aqueous Methylene Blue Using Bimetallic Fe-Cu NPs in Comparison with Fe NPs, *J. Mater. Environ. Sci*. **2021**, *12*, 42-54.
101. Sun, Y. P.; Li, X. Q.; Zhang, W. X.; Wang, H. P., A method for the preparation of stable dispersion of zero-valent iron nanoparticles. *Colloids Surfaces A: Physicochem. Eng. Asp.* **2007**, *308*, 60–66.
102. Chen, H.; Lee, J. H.; Kim, Y. H.; Shin, D. W.; Park, S. C.; Meng, X.; Yoo, J. B., Metallic copper nanostructures synthesized by a facile hydrothermal method. *J. Nanosci. Nanotechnol.* **2010**, *10*, 629–636.
103. Liu, A.; Zhang, W.X., Fine structural features of nanoscale zero-valent iron characterized by spherical aberration corrected scanning transmission electron microscopy (Cs-STEM). *Analyst*. **2014**, *139*, 4512–4518.
104. Jabeen, H.; Kemp, K. C.; Chandra, V., Synthesis of nano zerovalent iron nanoparticles - Graphene composite for the treatment of lead contaminated water. *J. Environ. Manage.* **2013**, *130*, 429–435.
105. Desalegn, B.; Megharaj, M.; Chen, Z.; Naidu, R., Green synthesis of zero valent iron nanoparticle using mango peel extract and surface characterization using XPS and GC-MS. *Heliyon*. **2019**, *5*, 1-9.
106. Wu, S.; Rajeshkumar, S.; Madasamy, M.; Mahendran, V., Green synthesis of copper nanoparticles using Cissus vitiginea and its antioxidant and antibacterial activity against urinary tract infection pathogens. *Artif. Cells, Nanomedicine Biotechnol.* **2020**, *48*, 1153–1158.

107. Sharma, C.; Kaur, M.; Choudhary, A.; Sharma, S.; Paul, S., Nitrogen Doped Carbon–Silica Based Cu(0) Nanometal Catalyst Enriched with Well-Defined N-moieties: Synthesis and Application in One-Pot Synthesis of 1,4-Disubstituted-1,2,3-triazoles. *Catal. Letters*. **2020**, *150*, 82–94.

108. Akbari, A.; Mohamadzadeh, F., New Method of Synthesis of Stable Zero Valent Iron Nanoparticles (Nzvi) by Chelating Agent Diethylene Triamine Penta Acetic Acid (DTPA) and Removal of Radioactive Uranium from Ground Water by using Iron Nanoparticle. *J. Nanostructures*. **2012**, *2*, 175–181.

109. Amin, M. T.; Alazba, A. A.; Shafiq, M., Adsorptive removal of reactive black 5 from wastewater using bentonite clay: Isotherms, kinetics and thermodynamics. *Sustain.* **2015**,*7*, 15302–15318.

110. Ayawei, N.; Ebelegi, A. N.; Wankasi, D., Modelling and Interpretation of Adsorption Isotherms. *J. Chem.* **2017**, (*2017*), 1-8.

111. Umpuch, C.; Sakaew, S., Removal of methyl orange from aqueous solutions by adsorption using chitosan intercalated montmorillonite. *Songklanakarin J. Sci. Technol.* **2013,***35*, 451–459.

112. MOGADDASI, F.; MOMEN, M.; HERAVI; BOZORGMEHR, M. R.; ARDALAN, P.; ARDALAN, T., Kinetic and Thermodynamic Study on the Removal of Methyl Orange From Aqueous Solution by Adsorption onto Camel Thorn Plant. *Asian J. Chem.* **2010**, *22*, 5093-5100.

113. Huang, Y. T.; Shih, M. C., Effect of linearized expressions of Langmuir equations on the prediction of the adsorption of methylene blue on rice husk. *Int. J. Sci. Res. Publ.* **2016**, *6*, 549-554.

114. Shahwan, T., Critical insights into the limitations and interpretations of the determination of ΔG^o, ΔH^o, and ΔS^o of sorption of aqueous pollutants on different sorbents. *Colloids Interface Sci. Commun.* **2021**, *41*, 100369.

115. Darwish, A. A. A.; Rashad, M.; AL-Aoh, H. A., Methyl orange adsorption comparison on nanoparticles: Isotherm, kinetics, and thermodynamic studies. *Dye. Pigment.* **2019,** *160*, 563–571.

116. AL-Aoh, H. A.; Yahya, R.; Jamil, M. M.; Radzi, M., Adsorption of methylene blue on activated carbon fiber prepared from coconut husk: isotherm, kinetics and thermodynamics studies. *Desalin. Water Treat.* **2014**, *52*, 6720–6732.

117. Wang, N.; Zheng, T.; Zhang, G.; Wang, P., A review on Fenton-like processes for organic wastewater treatment. *J. Environ. Chem. Eng*. **2016**, *4*, 762–787.

118. Nguyen, T. B.; Donga, C. H.; Huang, C. B.; Chena, C. W.; Hsiehc, S. L.; Hsiehd, S., Fe-Cu bimetallic catalyst for the degradation of hazardous organic chemicals exemplified by methylene blue in Fenton-like reaction. *J. Environ. Chem. Eng.* **2020**, *8*, 2-10.

119. Keenan, C. R.; Sedlak, D. L., Factors Affecting the Yield of Oxidants from the Reaction of Nanoparticulate Zero-Valent Iron and Oxygen, Environ. Sci. Technol. **2008**, *42*, 1262–1267.

120. Shahwan, T., Lagergren's Equation: Can Maximum Loading of Sorption Replace Equilibrium Loading? *Chem. Eng. Res. Des.* **2015**, *96*, 172–176.

121. Oboh, I. O.; Aluyor, E. O.; Audu, T. O. K., Second-Order Kinetic Model for the Adsorption of Divalent Metal Ions on Sida Acuta Leaves. *Int. J. Phys.Sci*. **2013**, *8* (34), 1722–1728.

122. Shahwan, T., Sorption Kinetics: Obtaining a Pseudo-Second Order Rate Equation Based on a Mass Balance Approach. *J. Environ. Chem. Eng.* **2014**, *2*, 1001–1006.

Appendix

Methyl Orange Calibration Curve

The spectrophotometer was used to obtain three calibration curves for the three solvents.

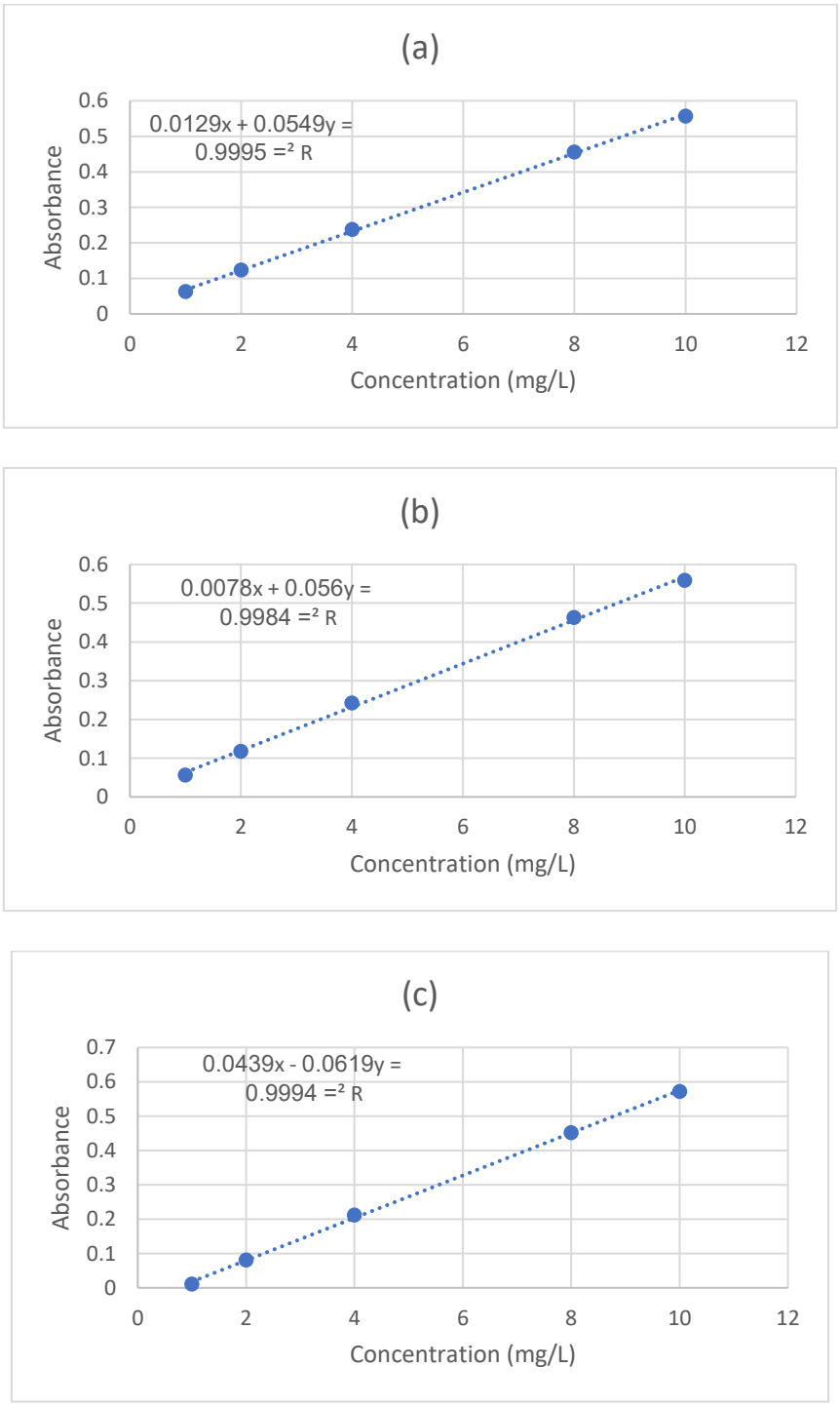

Figure A: Calibration curves for MO in: (a) W, (B) W-E, and (c) W-DMSO**.**